

Original Research

The Impact of Optical Undersampling on the Ca²⁺ Signal Resolution in Ca²⁺ Imaging of Spontaneous Neuronal Activity

Katarina D. Milicevic^{1,2}, Violetta O. Ivanova¹, Tina N. Brazil¹, Cesar A. Varillas¹, Yan M.D. Zhu¹, Pavle R. Andjus², Srdjan D. Antic^{1,*}

Academic Editor: Bettina Platt

Submitted: 23 August 2024 Revised: 3 October 2024 Accepted: 24 October 2024 Published: 21 January 2025

Abstract

Background: In neuroscience, Ca²⁺ imaging is a prevalent technique used to infer neuronal electrical activity, often relying on optical signals recorded at low sampling rates (3 to 30 Hz) across multiple neurons simultaneously. This study investigated whether increasing the sampling rate preserves critical information that may be missed at slower acquisition speeds. Methods: Primary neuronal cultures were prepared from the cortex of newborn pups. Neurons were loaded with Oregon Green BAPTA-1 AM (OGB1-AM) fluorescent indicator. Spontaneous neuronal activity was recorded at low (14 Hz) and high (500 Hz) sampling rates, and the same neurons (n = 269) were analyzed under both conditions. We compared optical signal amplitude, duration, and frequency. Results: Although recurring Ca²⁺ transients appeared visually similar at 14 Hz and 500 Hz, quantitative analysis revealed significantly faster rise times and shorter durations (half-widths) at the higher sampling rate. Small-amplitude Ca²⁺ transients, undetectable at 14 Hz, became evident at 500 Hz, particularly in the neuropil (putative dendrites and axons), but not in nearby cell bodies. Large Ca²⁺ transients exhibited greater amplitudes and faster temporal dynamics in dendrites compared with somas, potentially due to the higher surface-to-volume ratio of dendrites. In neurons bulk-loaded with OGB1-AM, cell nucleus-mediated signal distortions were observed in every neuron examined (n = 57). Specifically, two regions of interest (ROIs) on different segments of the same cell body displayed significantly different signal amplitudes and durations due to dye accumulation in the nucleus. Conclusions: Our findings reveal that Ca²⁺ signal undersampling leads to three types of information loss: (1) distortion of rise times and durations for large-amplitude transients, (2) failure to detect small-amplitude transients in cell bodies, and (3) omission of small-amplitude transients in the neuropil.

Keywords: intracellular calcium; neuropil; dendrites; cell nucleus; signal distortion; wide-field imaging; high-speed imaging; CCD camera

1. Introduction

Firing of an action potential (AP) often causes an influx of Ca²⁺ into the intracellular space. Via light-emitting Ca-binding molecules, one is thus capable of detecting APs by measuring light fluctuations in neurons [1-3]. Due to its substantial optical signals, Ca^{2+} imaging is used to monitor brain activity, spanning spatial scales from synapses and dendrites to individual cells and circuits. Ca²⁺ imaging is often used in a wide-field fluorescence-based approach that combines good spatiotemporal resolution with large fields of view [4]. Through sustained expansion of fluorescent reporters for neuronal activity [5], and indicator expression strategies [6,7], Ca²⁺ imaging analysis enables measurement and correlation of network dynamics with behavior [8]. One major feature of Ca²⁺ imaging is parallel recordings from many cells. Simultaneous registration of activity from multiple neurons improves the data robustness, and reduces the number of experimental trials required for obtaining significant differences between experimental groups. However, the number of recording sites is always in an indirect (inverted) proportion to the sampling rate. As the number of individual channels (neurons) increases, the sampling rate at which each channel (neuron) can be monitored decreases. What type of information is lost due to undersampling of optical Ca²⁺ transients? Before answering this question through experiments (Results section), we provide a brief overview of two popular Ca²⁺ imaging methods used in neuroscience.

In vivo two-photon calcium imaging is a method for registering neuronal activity in the brain of a living animal at the cellular or subcellular level. Main advantage of two-photon calcium imaging is high spatial resolution (<1 μm) and high-sensitivity fluorescence detection [9,10]. Objectives with moderate magnification are often employed, therefore the field of view is limited to up to 1 mm² [9,11]. Excitation wavelength in the infrared or near-infrared spectra, enables light to penetrate several hundred micrometers into the brain tissue. This is more effective than the wavelengths used in one-photon microscopy and provides the option for optical sectioning [12–14]. The focused spot is

¹Neuroscience Department, University of Connecticut Health, School of Medicine, Institute for Systems Genomics, Farmington, CT 06030, USA

²Center for Laser Microscopy, Institute of Physiology and Biochemistry 'Jean Giaja' , Faculty of Biology, University of Belgrade, 11000 Belgrade, Serbia

^{*}Correspondence: antic@uchc.edu (Srdjan D. Antic)

Table 1. In vivo two-photon multi-cell Ca²⁺ imaging—Sampling rates and major findings.

	Research Study	Sampling Rate	Selected Findings
1	Heintz et al. (2022)	6.07 Hz	Inhibitory microcircuits differently regulate the adaptation of pyramidal cells in the mouse visual cortex [18].
2	Liu et al. (2023)	10 Hz	Visual pathways transmit behaviorally relevant motion signals from selective visual areas to the brainstem, facilitating the plasticity of the optokinetic reflex behavior [16].
3	Ren et al. (2022)	28 Hz	During motor learning, acetylcholine regulates global and subtype-specific modulation of cortical inhibitory neurons [23].
4	Allen et al. (2017)	30 Hz	Local patterns of neocortical neuronal activity are globally coordinated [19].
5	Liu et al. (2019)	30 Hz	Different regions of the auditory cortex process sound onset and offset through parallel and spatially organized projections from the medial geniculate body, and are refined by specific intracortical connectivity [20].
6	Tang et al. (2020)	30 Hz	Layer 5 corticopontine neurons encode information related to sensory and motor tasks, and are crucial for task performance [17].
7	Benisty et al. (2024)	30 Hz	Correlations among neighboring neurons and between local and large-scale networks encode behavior [24].
8	Ferguson et al. (2023)	30 Hz	Interneurons that co-express vasoactive intestinal peptides participate in both state-dependent modulation of cortical activity and sensory context-dependent perceptual performance [25].
9	Gasselin et al. (2021)	30 Hz	Cell-type-specific nicotinic input disinhibits mouse barrel cortex during active sensing [26].
10	Musall et al. (2019)	30.9 Hz	During cognition, animals engage in a diverse array of uninstructed movements that influence neural activity [15].
11	Musall et al. (2023)	30.9 Hz	Different pyramidal neuronal types exhibit functionally distinct, cortex-wide neural dynamics that shape perceptual decisions [21].
12	Keller <i>et al.</i> (2020)	8–40 Hz	In the primary visual cortex, a canonical cortical disinhibitory circuit, consisting of inhibitory neurons producing vasoactive intestinal peptide and somatostatin, plays a role in contextual modulation [22].
13	Korzhova et al. (2021)	10 Hz	The neuronal network pathology seen in models of cerebral amyloidosis results from sustained aberrant activity in individual neurons [27].
14	He et al. (2017)	7.8 Hz	Sensory overactivity in the mouse model of fragile X syndrome is likely due to a defect in sensory adaptation within local neuronal networks [28].

scanned across the sample and the signals are collected with a photomultiplier tube. The sampling speed is limited by the scanning speed, thus resulting in the sampling frequency below 100 Hz [9,11]. Despite the relatively low sampling speed, it is fast enough to capture neuronal calcium activity during animal behavior [15–17]. Two-photon calcium imaging is employed to study neuronal networks and neuronal subtypes in various aspects of information processing [18-22]. Subcellular expression of genetically encoded calcium indicators (GECI) in different neuronal compartments (soma, axon, or dendrites) together with in vivo two-photon microscopy allows investigating calcium activity of these compartments separately in living animals [14]. A selection of two-photon calcium imaging studies conducted in living animals, the sampling rates employed, and the major findings, are presented in Table 1 (Ref. [15–28]).

Widefield calcium imaging is a practical method for measuring calcium activity across large brain regions in living animals using chemical indicators (Ca-sensitive dyes) or GECIs [11,29]. The widefield approach was successfully employed for studying brain circuitry and neuronal networks [24,30], cortex-wide activity in specific neuronal populations [19,21], and neuronal Ca²⁺ signaling during

behavior [31-33]. A key characteristic of widefield calcium imaging is its low temporal resolution [11,34], with sampling frequency typically ranging between 10 and 30 Hz (see Table 2, Ref. [19,21,23,24,30-32,35-39]). Two common approaches involve mesoscopic widefield imaging and widefield imaging using head-mounted systems [11,33]. Mesoscopic widefield imaging uses a low-magnification objective, thus enabling registration from a field of view as large as 100 mm² [21]. During imaging, the entire sample (brain) is exposed to the excitation light and the emission light is passed onto a high-sensitivity camera (Charged-Coupled Device (CCD), or Complementary Metal-Oxide Semiconductor (CMOS)) via a microscope. While typical camera resolutions encompass approximately 512 × 512 pixels; pixel binning is frequently used, leading to further spatial resolution reduction [11]. Due to its low spatial resolution, this technique cannot resolve single cell activity; the signal detected from a single pixel represents the integration of both somatic and neuropil activity [29,40]. Different approaches have been developing to overcome this issue. For example, restricted expression of GCaMP6 to a small cell population, or specific cell compartments, produces a robust transcranial signal and allows for investiga-



Table 2. In vivo wide-field multi-cell Ca²⁺ imaging – Sampling rates and major findings.

	Research Study	Sampling Rate	Selected Findings
1	Benisty et al. (2024)	10 Hz	Correlations among neighboring neurons and between local and large-scale networks
			encode behavior [24].
2	Wang et al. (2024)	10 Hz	Dynorphin peptidergic signaling in the prefrontal cortex suppresses defensive behav-
			ior by altering network states [31].
3	Lohani et al. (2022)	10 Hz	Functional reorganization of cortical networks, and fluctuations in behavior, use
			acetylcholine-mediated spatially-heterogeneous signals [36].
4	Ishino et al. (2023)	10 Hz	Adaptive and robust pursuit of uncertain reward to ultimately obtain more reward
			is enabled by the cooperation between the dopamine error signal and the reward
			prediction error signal [32].
5	Smith et al. (2018)	15 Hz	Structured long-range network correlations that guide the formation of visually
			evoked distributed functional networks, are established by local connections in early
			cortical circuits [30].
6	Heiss et al. (2024)	15 Hz	Lateral hypothalamus contains two distinct populations of $CaMKII\alpha$ neurons that
			regulate locomotion and wakefulness [35].
7	Allen et al. (2017)	15 Hz	Local patterns of activity in the cortex are globally coordinated [19].
8	Piantadosi et al. (2024)	20 Hz	Compulsive behavior is enhanced/promoted by hyperactivity of indirect pathway-
			projecting spiny projection neurons [37].
9	Manning et al. (2023)	20 Hz	Lateral orbitofrontal cortex has distinct roles in pathophysiology and treatment of
			different perseverative behaviors in obsessive-compulsive disorder [38].
10	Ren et al. (2022)	29.98 Hz	Acetylcholine regulates global and subtype-specific modulation of cortical inhibitory
			neurons during motor learning [23].
11	Liu et al. (2021)	29.98 Hz	During hippocampal sharp-wave ripples, hippocampus and large-scale cortical activ-
			ity engage in selective and diverse interactions that support various cognitive func-
			tions [39].
12	Musall et al. (2023)	30 Hz	Different pyramidal neuronal types exhibit functionally distinct, cortex-wide neural
			dynamics that shape perceptual decisions [21].

tion of specific neural pathways or specific neuronal subtypes activity in certain conditions [6,41,42]. A smaller field of view leads to enhanced spatial resolution, allowing for differentiation of events originating from individual neurons [32,35]. On the other hand, widefield Ca²⁺ imaging with head-mounted systems enables monitoring of neuronal Ca²⁺ activity across brain areas (e.g., 1 mm²) in freely moving animals [33]. Calcium imaging videos obtained in moving animals have challenging noise properties, including white noise and motion artifacts, which must be corrected [43,44]. Table 2 summarizes recent biological findings using widefield calcium imaging.

Since Ca²⁺ transients are inherently slow, it is likely that Ca²⁺ imaging sessions using low optical sampling speeds in the range 3–30 Hz should capture the essence of Ca²⁺ signaling entirely. In this study, we investigate whether faster sampling speeds can capture valuable information that slower speeds might miss. To this end, we recorded spontaneous activity of neurons at two speeds, slow (14 Hz) and fast (500 Hz). Visual observations of recorded spontaneous Ca²⁺ signals did not indicate any significant differences between 14-Hz and 500-Hz recordings. However, quantitative analysis reveals that spontaneous calcium events recorded at 500 Hz had faster risetimes and their duration (half-width) has been significantly

shorter in comparison to the 14 Hz data acquisition mode. At 500 Hz, we detected the presence of small-amplitude short-duration spontaneous Ca2+ events that were not detectable at 14 Hz. At 500 Hz sampling rate, these smallamplitude Ca²⁺ transients were particularly prominent in the neuropil composed of dendrites and axons, but were undetectable in the nearby cell bodies, despite both regions of interest (ROIs) being recorded at the same moment of time. Our study reveals that Ca²⁺ undersampling can distort the rise-time and duration of large-amplitude Ca²⁺ transients and prevent detection of small-amplitude Ca²⁺ transients in both the cell body and especially the neuropil. In summary, Ca²⁺ signal undersampling results in a three-fold loss of information: (1) severe distortions in the rise-time and duration of large-amplitude transients, (2) loss of smallamplitude transients in the cell body, and (3) loss of smallamplitude transients in the neuropil.

2. Methods

2.1 Primary Cortical Neuronal Cell Culture

Primary neurons were isolated from the cortices of newborn pups (P0-P1) of C57BL/6 mice, which were anesthetized by hypothermia and decapitated. In brief, isolation of cortices was done in dissecting medium (DM) composed of HBSS without calcium and magnesium (GibcoTM,



cat. No. 14175079, Thermo Fisher Scientific, Grand Island, NY, USA), 1 mM sodium pyruvate, 0.02% (w/v) glucose, and 10 mM HEPES (GibcoTM, cat. No. 15630-080, Thermo Fisher Scientific, Grand Island, NY, USA). After washing in DM three times, cortices were enzymatically digested at 37 °C in the water bath in 1 mg/mL trypsin in DM (freshly dissolved before this step; cat. No. T6567, Sigma-Aldrich, St. Louis, MO, USA) for 20 min with occasional mixing. Loosened tissue was allowed to settle at the bottom of the tube, then rinsed three times in DM, followed by three washes in temperature-equilibrated plating medium (PM) composed of Dulbecco's Modified Eagle Medium/Nutrient Mixture F-12 (Gibco™, Thermo Fisher Scientific, USA, cat. No: 11320033), 10% FBS, 0.02% (w/v) glucose, and 10 μg/mL gentamicin (cat. No. G1272-10ML, Sigma-Aldrich, St. Louis, MO, USA). Cortices were gently mechanically homogenized in 1 mL of PM using a 1000 µL pipette tip and incubated for 5 min at room temperature to allow larger pieces to settle on the bottom of the tube. Cells in the suspension (without larger tissue pieces) were counted and ~60,000 cells/well was plated onto 12 mm round glass coverslips (previously coated with poly-1-ornithine 50 µg/mL (cat. No. P4957-50ML, Sigma-Aldrich, St. Louis, MO, USA)) in 24-well plates. Two hours after plating the cells, the maintenance medium (MM) was added. MM was composed of BrainPhys Neuronal Medium (cat. No. 05790, Stemcell Technologies, Vancouver, BC, Canada), 2% SM1 Neuronal Supplement (cat. No. 05711, Stemcell Technologies, Vancouver, BC, Canada), 2 mM GlutaMAX (GibcoTM, cat. No. 35050-061, Thermo Fisher Scientific, Grand Island, NY, USA), and 10 µg/mL gentamicin (cat. No. G1272-10ML, Sigma-Aldrich, St. Louis, MO, USA). Primary cortical neurons were grown in a humidified atmosphere of 5% $CO_2/95\%$ air at 37 °C. Half of the medium was replaced with fresh MM 24 hours after isolation. On the third day after plating, half of the medium was replaced with fresh MM, enriched with cytosine β -d-arabinofuranoside hydrochloride (final concentration, 1 µM; cat. No. C6645-25MG, Sigma-Aldrich, USA). Every third day, the half of the medium was exchanged for fresh MM. Neurons were imaged after growing 11 days in vitro (DIV), at which stage they were able to generate APs.

2.2 Electrical Recordings

Neurons on glass coverslips were placed in the optical imaging chamber of an Olympus BX51WI microscope (SN OL56320, Olympus BX51WIF, Tokyo, Japan). The chamber was perfused with warm artificial cerebrospinal fluid (ACSF; 34 ± 1 °C) with the following composition (in mM): 125 NaCl, 26 NaHCO₃, 10 glucose, 5 KCl, 1.26 KH₂PO₄, 1.2 CaCl₂ and 2 MgSO₄ (pH 7.4, osmolality ~300 mOsm/kg). The ACSF was bubbled with 95% O₂/5% CO₂. Patch pipettes (resistance ~7 M Ω) were pulled from borosilicate glass with filament (outer diameter 1.5 mm, cat. No. G150F-3, Warner Instruments, Holliston, MA,

USA) and filled with intracellular solution containing (in mM): 135 K-gluconate, 2 MgCl₂, 3 Na₂-ATP, 10 Na₂-phosphocreatine, 0.3 Na₂-GTP, and 10 HEPES (pH 7.3, adjusted with KOH). The Ca²⁺-sensitive dye OGB1 (Oregon GreenTM 488 BAPTA-1, cat. No. O6806, Thermo Fisher Scientific), was dissolved directly in the intracellular solution. Electrical recordings were obtained and stored using a Multiclamp 700B amplifier and Clampex 9.2 software (Molecular Devices, Sunnyvale, CA, USA).

2.3 Neuron Labeling with OGB-1 Hexapotassium Salt

Primary cortical neurons were loaded with OGB1 by patching with intracellular solution containing 25 μM of OGB1. The dye diffused freely into the cytoplasm, with good optical signals detected in the cell body within 10–15 minutes of whole-cell patching. Between 20 and 30 minutes after the whole-cell break-in, dendrites and axons were adequately filled with the fluorescent dye.

2.4 Neuron Labeling with OGB1-AM

Manufacturer's instructions were followed in the preparation of the OGB1-AM stock solution (Invitrogen, USA, cat. No: O6807). Primary cortical neurons were extracellularly loaded with 2.67 μ M OGB1-AM for 20 min at 37 °C. After incubation, coverslips were placed in MM at 37 °C for 10 minutes to allow dye de-esterification, and removal of excess dye.

2.5 Optical Recordings

Coverslips with OGB1-AM-loaded neurons were transferred to the Olympus BX51WI microscope, perfused with oxygenated ACSF. The OGB-1 fluorophore was excited using a 470 nm light emitting diode, LED (pE, CoolLED, Andover, UK), excitation filter of 480/40 nm, dichroic filter of 510 nm, and emission filter of 535/50 nm. Max power of the LED illumination at 100% was 14 mW/mm². Images projected onto an 80×80 -pixel CCD camera (NeuroCCD-SMQ; RedShirtImaging, Decatur, GA, USA) using $10 \times (0.3 \text{ NA})$ and $40 \times (0.8 \text{ NA})$ water immersion objectives. Videos were sampled at 72 ms per frame (14 Hz), or 2 ms per frame (500 Hz).

2.6 Field Selection

Two primary criteria were used to select the experimental field of view. First, infrared differential interference contrast (IR-DIC) video microscopy was used to identify areas with groups of neurons displaying smooth, healthy membranes. Each field typically contained 8–23 neurons. Low-density regions on the coverslip were avoided. Second, neuronal spontaneous activity was monitored at a sampling rate of 14 Hz for three 15-second sweeps. If fewer than three cells were active during the 45-second ($3 \times 15 \text{ s}$) observation period, the X-Y translator was used to relocate to another position on the coverslip. No additional biases were applied for field selection in this study.



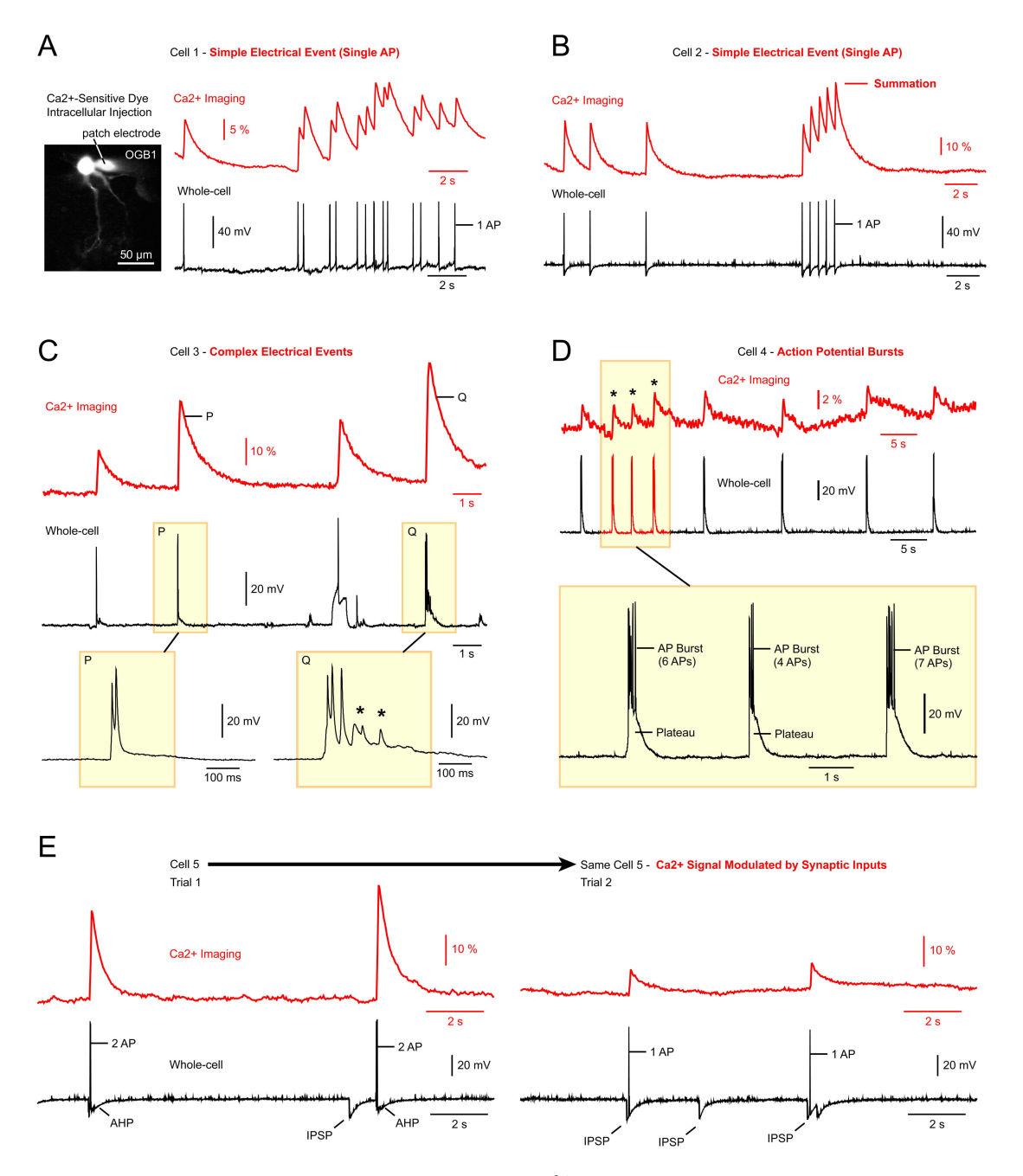


Fig. 1. Great variability of electrical signals underlying optical Ca²⁺ transients. Each panel (A–E) represents a dual electrical (sampling rate of 5 kHz) and optical recording (camera frame rate of 28 Hz) from a different neuron. (A) A cultured neuron was injected with a membrane impermeable Ca²⁺-sensitive dye, OGB1 (Oregon GreenTM 488, BAPTA-1). Spontaneous activity is then recorded in two ways: optically (red), and electrically (black trace). Simple electrical events (action potentials, APs) translate into optical signals where each peak marks the timing of an AP. The scale bar = 50μm. (B) Same experimental setup but a different cell. Reduced time intervals between APs cause temporal summation of Ca²⁺ transients. (C) Complex voltage waveforms (black) generate optical Ca²⁺ transients (red trace). If only optical data were available, it would be impossible to predict the type of electrical signaling (P and Q) behind each optical transient. (D) Simple Ca²⁺ transients suggest that each Ca²⁺ event was caused by an AP. However, patch electrode recording (whole-cell) revealed that each event is actually caused by a burst of APs (asterisk). Although the number of AP in the "AP burst", and duration of the underlying "Plateau" potential, both vary significantly, this is not reliably reflected in the Ca²⁺ imaging data (red trace). (E) Two experimental trials obtained in the same cell, only seconds apart. In the second trial (Trial 2), a spontaneous inhibitory postsynaptic potential (IPSP) reduces the optical signal amplitude. In the absence of a whole-cell recording, the Ca²⁺ imaging technique cannot determine if an AP was affected by: (i) synaptic input, (ii) neuromodulation, (iii) phototoxicity, or (iv) some other loss of cell's integrity. Asterisks (*) indicate subtreshold activity. AP, action potential.



2.7 Data Analysis

Optical traces were processed and analyzed using Neuroplex, Clampfit, and MATLAB software (Neuroplex: version 9.8.1, RedShirtImaging LLC, Decatur, GA, USA; Clampfit: Version 11.3.0.02, Molecular Device. LLC, San Hose, CA, USA; MATLAB Software: Version R2024a, MathWorks, Inc., Natick, MA, USA). The Neuroplex data acquisition and analysis software (version 9.8.1, RedShirtImaging, Decatur, GA, USA) was used for: (1) spatial averaging, (2) exponential subtraction, and (3) filtering. The values for the low-pass Gaussian filter and the high-pass RC filter are indicated in the figures. Averaged intensity of the region of interests (ROIs) containing neuronal cell bodies or neuropil were used in the analysis. Amplitudes of optical signals are expressed as $\Delta F/F$ (F is the resting fluorescent signal intensity at the beginning of the optical trace (baseline), while ΔF is the intensity shift from the baseline fluorescence during a spontaneous electrical activity event. Clampfit software (version 10.2.2. for Windows, Molecular Devices, San Jose, CA, USA) was used for interpolation of traces to a higher sampling rate, determination of the amplitude, half-width, and rise-time of spontaneously occurring neuronal activity events was done in Clampfit software (version 10.2.2. for Windows, Molecular Devices, San Jose, CA, USA). That is, optical traces obtained at 14 Hz rate were first interpolated to 140 Hz and then quantified. Results are presented as average values \pm the standard error of the mean (SEM), unless otherwise stated. The optical signal rise-time from 10% to 90% of the maximum value was quantified.

Unbiased selection of ROIs was conducted using an open-source software, EZcalcium [45]. EZcalcium v3.0.2 was downloaded from the GitHub site (https://github.com /porteralab/EZcalcium) and added to the MATLAB path. MATLAB 2024a Update 5 24.1.0.2653294 for Win64 was used. Automated ROI Detection option was used to detect ROI corresponding to individual neurons. Parameters for ROI Detection were kept the same for all analyzed fields of view. Using ROI Refinement option traces were extracted and "inferred" traces were used for the Ca²⁺ event parameter analysis. "Manual Analysis" refers to a manual selection of ROIs using a kernel function in Neuroplex, and export of optical traces. A custom-built Jupyter Lab routine was employed to accomplish three measurements: (1) number of Ca transients crossing the arbitrary threshold, (2) their peak amplitudes, $\Delta F/F$ (in %), and (3) half-widths (in ms). Same threshold for event detection was set for the same trace extracted with either EZcalcium or Manually. Statistical analysis was done using paired and unpaired student's t-tests in GraphPad Prism for Windows, version 10.2.3 (GraphPad Software, Inc., San Diego, CA, USA).

3. Results

The depolarization of the neuronal membrane leads to the opening of Ca²⁺-permeable channels and consequent influx of Ca^{2+} ions. An increase in cytosolic Ca^{2+} concentration can be detected by optical recording [1]. This phenomenon has been widely utilized in numerous studies to monitor activity across multiple neurons simultaneously, using relatively low optical sampling rates, e.g., 3–30 Hz [8,46,47]. Although not always explicitly stated, the in vivo studies interpret Ca^{2+} imaging signals as indicative of AP firing. To investigate the nature of electrical signaling underlying neuronal Ca^{2+} transients, we performed simultaneous optical and electrical recordings in cultured neurons experiencing spontaneous activity. Neurons (n = 9) were loaded with the Ca^{2+} -sensitive dye Oregon GreenTM 488 BAPTA-1 (OGB1) via a patch pipette using the whole-cell configuration (Fig. 1A, image).

3.1 Simple Electrical Events

In the simplest scenario, commonly assumed by researchers employing in-vivo Ca²⁺ imaging technique, each AP corresponds to an individual Ca²⁺ transient observed in the optical trace (Fig. 1A, traces). It is well established that rapid AP firing causes Ca2+ transients to overlap and merge at their bases (Fig. 1B). As the AP train progresses, late spikes occur against an already elevated Ca²⁺ baseline, resulting in an increased amplitude of the optical signal. This effect arises from a gradually accumulating residual Ca²⁺, due to both a slow clearance rate from the cytosol and the slow OFF rate of the fluorescent indicator. Consequently, the optical Ca²⁺ transients exhibit summation in the recorded traces (Fig. 1B, summation). However, simple electrical events, in the form of individual APs void of any underlying significant depolarizations (Fig. 1A,B, wholecell), are rare.

3.2 Complex Electrical Events

In many instances, neuronal electrical signaling is more intricate and not limited to simple AP firing. Instead, APs are interspersed with various other depolarizing signals. Such complex electrical waveforms were observed in every neuron examined (n = 9), clearly demonstrating that optical signals alone are insufficient to distinguish between different types of neuronal electrical activities. For instance, the optical transients labeled P and Q appear quite similar, yet the electrical "Q" event encompasses a significant amount of subthreshold activity (Fig. 1C, asterisks). Additionally, simple optical transients (Fig. 1D, red trace, asterisks) often result from complex AP bursts, with highly variable number of APs per burst (Fig. 1D, AP Burst), and plateau depolarizations at the base of the burst (Fig. 1D, Plateau). Furthermore, the amplitude of optical signals in Ca²⁺ imaging experiments offers limited insight, as it is frequently influenced by natural factors, such as synaptic inputs (Fig. 1E) and neuromodulation, as well as by artifacts including cell health, and variations in optical sensitivity.

In summary, interpreting Ca²⁺ imaging data is challenging without concurrent measurements of neuronal



membrane potential (Fig. 1). We will next examine how the sampling rate influences the interpretation of Ca²⁺ traces.

3.3 Undersampling of Ca²⁺ Signals

Using a 40× objective lens, we recorded Ca²⁺ transients from 8 to 23 neurons per sweep (Fig. 2E). We used low illumination intensity (less than 10% LED power, 1.4 mW/mm²) allowing us to obtain multiple optical sweeps from the same field of view. Low illumination intensity is critical when investigating neuronal physiology before and after acute treatment with different agents and conditions (e.g., electrolytes, drugs, temperature, radiation, etc.). Two consecutive sweeps, each with a duration of 15 seconds, are shown in Fig. 2A,B. An average number of 2.5 \pm 0.2 good-sized (amplitude exceeding 3% Δ F/F) & slow (duration exceeding 100 ms at half amplitude) Ca²⁺ transients per recording trial was detected (n = 36 trials, 8 coverslips), which is equivalent to 9.6 \pm 0.9 Ca²⁺ events per minute. The presence of simultaneous large-amplitude Ca²⁺ transients in multiple neurons (Fig. 2A,B) indicates robust synaptic connections among them and synchronized neuronal network. To identify information lost due to undersampling, we conducted "dual sampling rate" experiments within the same field of view (FOV) containing multiple cultured neurons (Fig. 2E). Namely, while keeping the x-y position and focus unchanged, optical recordings were first conducted at 14 Hz (two sweeps, 15 seconds each) and then at 500 Hz (two sweeps, 15 seconds each). In this way, spontaneously occurring Ca²⁺ optical signals were sampled from the same cell at two different rates: 14 Hz and 500 Hz (Fig. 2A-D). Based solely on a visual inspection of traces on a slow time scale, no discernible type of Ca²⁺ signal present at 500 Hz was lost at 14 Hz. Our initial visual analysis suggested that the slower 14 Hz rate minimally distorts the Ca²⁺ waveforms (Fig. 2, compare panels A,B vs. panels C,D). Superimposing unfiltered optical traces sampled at 14 Hz and 500 Hz revealed nearly identical waveforms in both recording scenarios (Fig. 3). For instance, we recorded from "Cell 1" at 14 Hz sampling rate (Fig. 3A) and then at 500 Hz (Fig. 3B). Using a red rectangle, we selected one recurring Ca²⁺ waveform that appeared in several subsequent recordings from the same cell. Superimposing these repetitive Ca²⁺ transients at two sampling rates showed marked similarities (Fig. 3C), suggesting that the sampling rate had minimal impact on the waveform. Additional waveforms marked with red and blue rectangles also appeared very similar at both sampling rates. Dual rate recordings, sequential 14 Hz and 500 Hz, described in Figs. 2,3 were obtained from 269 neurons.

Six out of the 269 neurons recorded for 60 seconds total, did not show any spontaneous Ca²⁺ transients. In the remaining 263 neurons, we identified at least 39 neurons with very similar waveforms at both sampling rates (Figs. 2,3). Visual inspection concluded that in a sizable number of spontaneously active neurons loaded with high-

affinity Ca^{2+} indicator OGB1-AM (Kd \sim 0.2 μ M), undersampling of Ca^{2+} optical signals causes minimal loss of information.

Two factors may be responsible for this result: (1) slow dynamics of the Ca^{2+} indicator, and (2) slow biological signals underlying the observed Ca^{2+} transients. (1) With low-affinity Ca^{2+} indicators (Kd >10 μ M), differences in kinetics are detectable between recordings at 5 kHz versus 20 kHz [48]. Therefore, the similarity in Ca^{2+} signal kinetics observed at 14 Hz and 500 Hz suggests that our Ca^{2+} -indicator (OGB1) exhibits slow dynamics due to its low Kd (~0.2 μ M). (2) The observed electrical events may also inherently be slow, such as those generated by glutamate-mediated dendritic plateaus, which are known to produce long-lasting slow-decaying Ca^{2+} transients lasting over 1 second [49,50].

Why opt for a slower rate? Opting for a slower rate offers several advantages. Firstly, it places less strain on the imaging system, resulting in fewer instances of computer crashes and smaller data file sizes. More significantly, it reduces strain on neurons within the FOV. With 20 times less intense illumination, there is a corresponding 20-fold reduction in photodamage.

3.4 Focus on the Differences between 14 Hz and 500 Hz

Our data suggested that large-size long-duration Ca²⁺ transients exhibit similar waveforms when recorded at either 14 Hz or 500 Hz (Figs. 2,3). If large and slow transients are captured equally-well at both sampling rates, there is a possibility that faster transients are not captured by the slower rate. We shifted our attention from large and slow transients to small-amplitude, short-duration Ca²⁺ transients. Between two consecutive Ca²⁺ signals (Fig. 4B, vellow rectangle) we detected small-amplitude transients, barely emerging above the baseline noise (Fig. 4C, arrows). For display in Fig. 4B, we selected 3 non-neighboring neurons (Cells 1-3, Fig. 4A,B), each providing evidence that small-amplitude short-duration Ca²⁺ transients are discernible in 500 Hz recording sessions (Fig. 4B, arrows), but not easily discernible with the 14 Hz sampling rate. We examined 16 multi-cell recording sessions obtained at both sampling rates. In these sessions, we found 83 neurons in which small and sharp Ca²⁺ optical signals appeared at 500 Hz but could not be discerned at the 14 Hz sampling speed.

3.5 Sharp Transients in the Neuropil

Unexpectedly, we found that ROIs positioned over a visual field areas involving dendrites and axons (neuropil) produced more frequent small and sharp Ca²⁺ events compared to ROIs selected on the cell bodies (somata) of neighboring neurons (Fig. 5A). In the illustrative example, one ROI (ROI-1) was selected on the neuropil, while four ROIs (ROI-2 to ROI-5) were positioned on the cell bodies of the neurons surrounding the neuropil (Fig. 5B). The idea was that electrical transients in one of these neurons might prop-



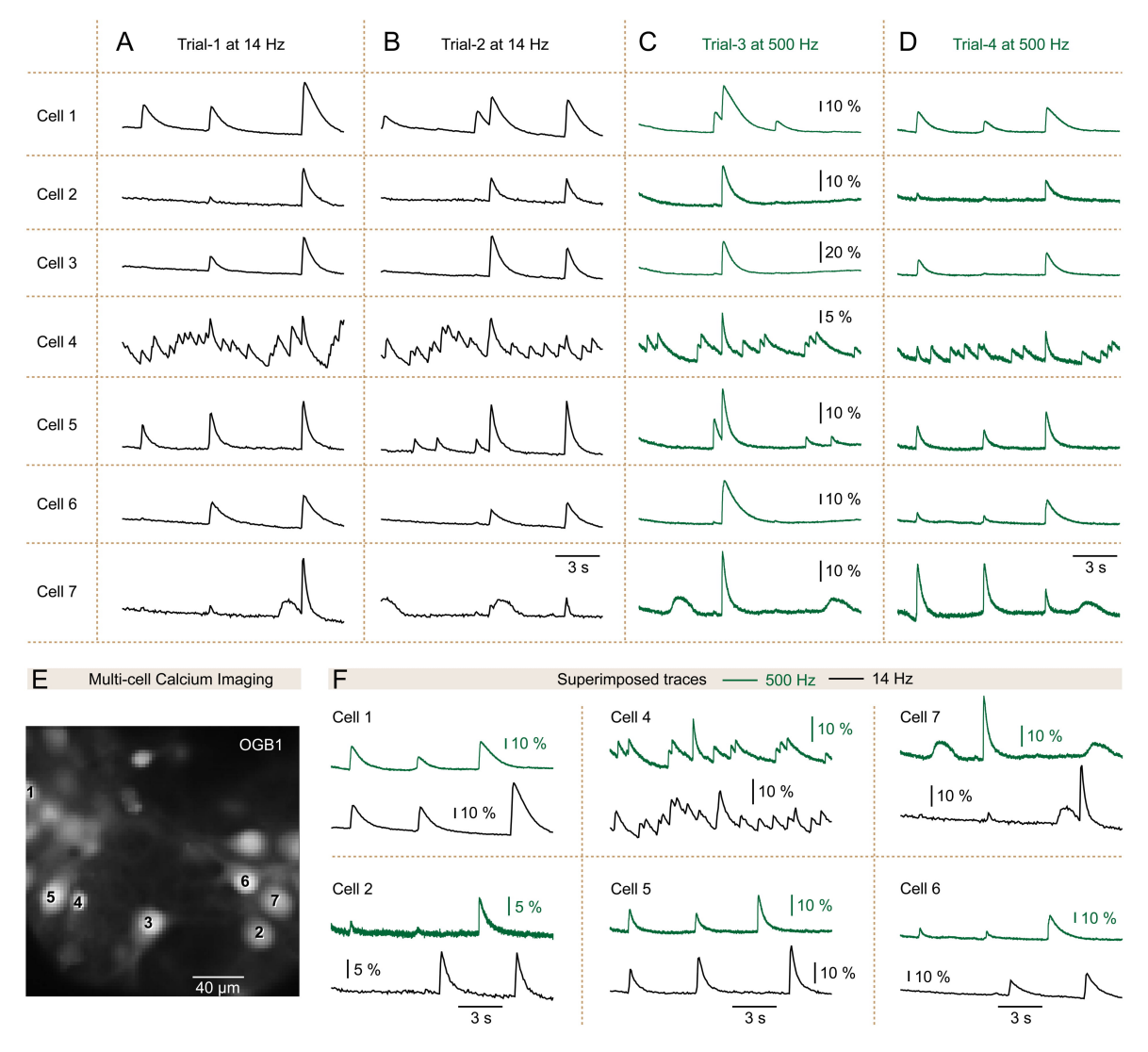


Fig. 2. Information about the optical Ca^{2+} transients is preserved with the 14 Hz-frame rate. Ca^{2+} imaging was conducted to observe the spontaneous activity of seven neurons (Cell 1 to Cell 7) across four experimental trials (from Trial-1 to Trial-4). (A) In Trial-1, a 72 ms sampling interval (sampling rate of 14 Hz) was utilized. (B) Similar to Trial-1, with the exception of a new recording trial captured 20 seconds later (Trial-2). (C) Identical to Trial-2, but with the sampling interval set to 2 ms (camera frame rate of 500 Hz). (D) Analogous to Trial-3, with another recording sweep taken 20 seconds later (Trial-4). (E) The field of view illustrates the neurons observed in Trials A–D. The scale bar = 40 μ m. (F) Traces from the same cell are overlaid to compare Ca^{2+} transients captured at a 2 ms sampling rate (green) with those captured at a 72 ms sampling rate (black). OGB1, Oregon GreenTM 488, BAPTA-1.

agate into the neuropil, allowing the optical signatures of the same electrical event to be recorded in two places simultaneously.

For example, propagating AP waveforms can be recorded both in the neurite and the cell body simultaneously [51]. Indeed, one of the cell bodies marked by ROI-2 exhibited simultaneous Ca²⁺ transients with the neuropil marked by ROI-1 (Fig. 5D, red vertical stripes "q" and "p") suggesting that the mechanism behind this result is either: [i] an AP backpropagation (from soma into dendrite), [ii] orthodromic propagation (from soma into axon), or [iii] antidromic AP propagation. In each case [i–iii], one AP is "visible" in both soma and neurite [51]. Similarly, the cell

body marked by ROI-4 exhibited simultaneous Ca²⁺ transients with the neuropil ROI-1 (Fig. 5D, red stripe "r"), and the cell body marked by ROI-8 exhibited simultaneous Ca²⁺ transients with the neuropil ROI-6 (Fig. 5E,F, green stripes "s" and "t").

In addition to these large-amplitude Ca²⁺ events, we identified several small-amplitude short- duration Ca²⁺ signals that were exclusive to the neuropil. The Ca²⁺ signals obtained in the neuropil ROI-1 (Fig. 5B, ROI-1) contained small and sharp Ca²⁺ transients that were not discernible in the nearby cell bodies (ROI-2 to ROI-5) (Fig. 5D, arrows). Similarly, the Ca²⁺ signals obtained in the neuropil ROI-6 (Fig. 5C, ROI-6) contained small and sharp Ca²⁺ transients that were not discernible in



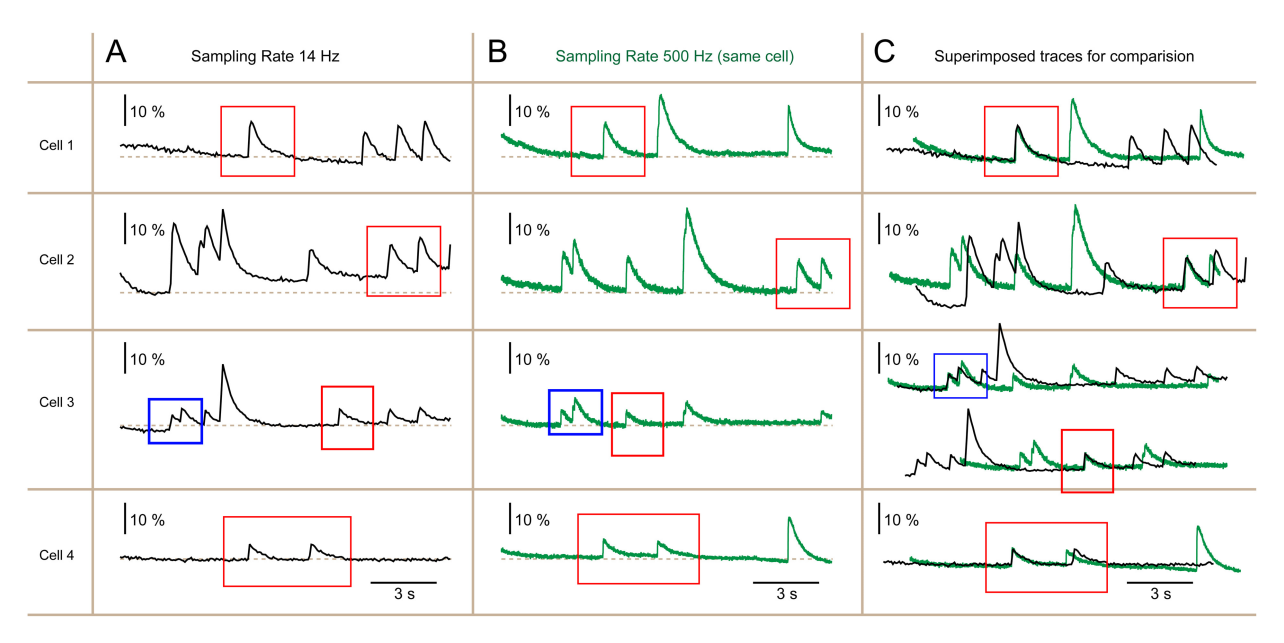


Fig. 3. Information about Ca²⁺ **transients is preserved with the 14 Hz frame rate.** (A) Ca²⁺ imaging was conducted to observe the spontaneous activity in four neurons simultaneously, employing a sampling rate of 14 Hz. (B) Similar to Panel A, apart from a new recording sweep taken approximately 20 seconds later, utilizing a faster sampling rate of 500 Hz. (C) Traces originating from the same cell are extracted from (A,B) and overlaid in (C) to compare Ca²⁺ transients captured at 500 Hz (depicted in green) with those captured at 14 Hz (depicted in black) sampling rates. Red and blue boxes highlight physiological events demonstrating nearly identical temporal dynamics at two distinct sampling rates.

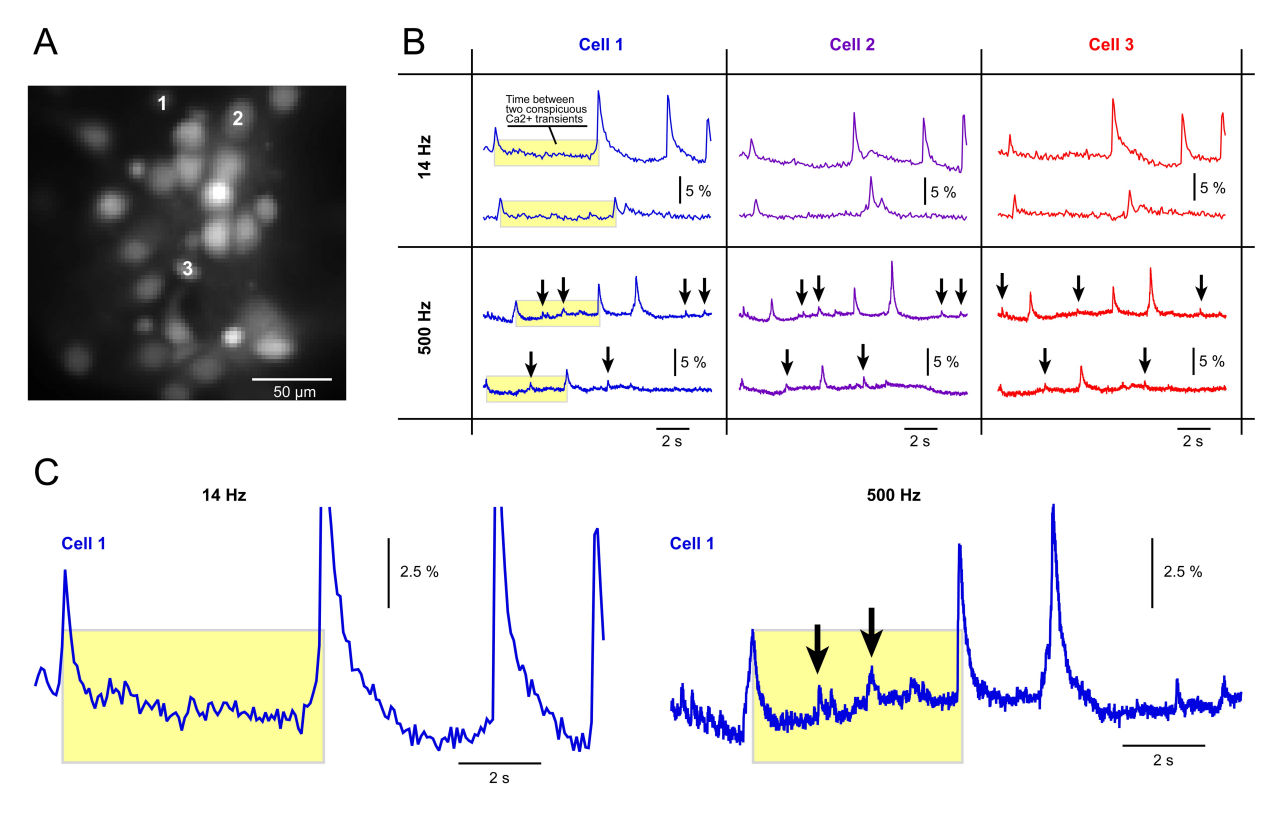


Fig. 4. Small-amplitude short-duration Ca^{2+} transients require a faster sampling rate. (A) Primary neurons bulk-loaded with a Ca^{2+} sensitive dye OGB1-AM and projected onto a fast CCD camera. The scale bar = 50 μ m. (B) Optical recordings of spontaneous Ca^{2+} activity from three cell bodies (soma). In each cell, two recordings were first captured at 14 Hz, then followed by two traces captured at 500 Hz sampling rate. Arrows mark small and narrow Ca^{2+} transients, which are poorly represented in traces obtained at 14 Hz. (C) Two traces from *B* are shown here on an expanded time scale. CCD, Charged-Coupled Device.

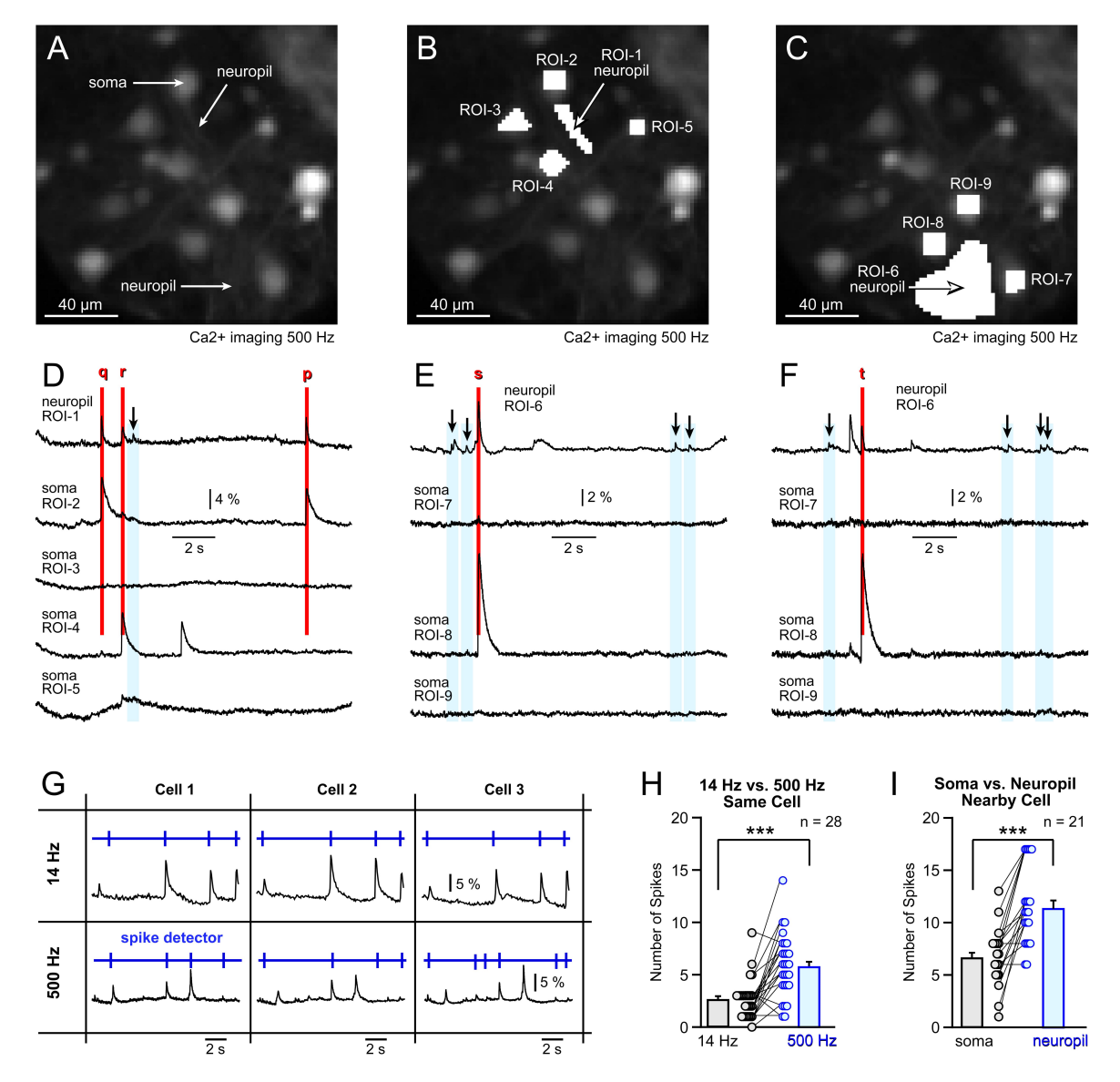


Fig. 5. Small and fast Ca²⁺ **transients are more often found in the neuropil.** (A) Primary neurons bulk-loaded with a Ca²⁺ sensitive dye OGB1-AM and projected onto a fast CCD camera at 500 Hz frame rate. Neuronal cell body (soma) and two sections rich with neuropil (dendrites & axons) are marked by labels. (B) Region of interest (ROI-1) is selected in the area with no neuronal cell bodies, where dendrites and axons (neuropil) are the only Ca²⁺ signal-producing structures. On the other hand, the ROIs 2–5 are selected over the neuronal cell bodies. (C) New ROIs are selected, with ROI-6 covering the neuropil, while ROIs 7–9 covering cell bodies of nearby neurons. The scale bar is 40 μm. (D) Optical signals from ROIs 1–5 marked in (B), reveal sharp Ca²⁺ transients in the neuropil. Arrows and blue rectangles mark sharp optical transients restricted to the neuropil only. (E) Optical signals from ROIs 6–9 marked in (C). The neuropil area (ROI-6) exhibits several sharp Ca²⁺ transients (arrows) which are not present in the cell bodies of the neighboring cells (ROIs 7, 8 and 9). (F) Multi-cell optical recording shown in the previous panel (E) was repeated 20 seconds later, using the same selection of ROIs. Again, sharp Ca²⁺ transients are enhanced in the neuropil area (ROI-6). (G) Detection of spikes using a *threshold search* function in Clampfit (cartoon illustration). (H) Spike count per 15-s-trace obtained in the same cell (same neuron) at two sampling frequencies. (I) Spike count per a 15 s-trace obtained in the neuropil versus the neighboring cell body, at 500 Hz optical sampling rate.

*** indicate p < 0.001.

sients not discernible in the nearby cell bodies (ROI-7 to ROI-9) (Fig. 5E,F, arrows). Visual inspection of 16 multicell recording sessions at 500 Hz revealed 21 neuropil areas (neuropil ROIs) exhibiting small and sharp Ca²⁺ transients that were not discernible in simultaneous 500 Hz record-

ings from the nearby cell bodies (n = 21). We concluded that small and sharp Ca^{2+} transients are more common in the neuropil compared to the cell body.

We analyzed optical traces obtained from the same neuron at two sampling frequencies, 14 Hz and 500 Hz.



Each trace in this analysis was extracted from the cell body (Soma ROI). Traces were exponentially subtracted and filtered (14 Hz recordings: High pass RC (0.1 Hz) Tau; 500 Hz recordings: Low pass Gaussian (44 Hz), High pass RC (0.1 Hz) Tau (10)). Exported traces were opened in ClampfitTM and Ca²⁺ transients (events) were counted manually (Fig. 5G, blue raster plot above the trace). In total, 29 pairs of dual-frequency recordings were analyzed in 4 different fields of view. A greater number of spikes was consistently detected at 500 Hz compared to 14 Hz in the cell bodies of 29 neurons (n = 29). This difference was statistically significant, as indicated by a paired t-test (p < 0.0001) (Fig. 5H, asterisks). These data indicate that spike detection is more efficient at higher sampling rates.

We used 500 Hz traces to compare a neuropil ROI (e.g., ROI-1, ROI-6) with an adjacent soma ROI (e.g., ROI-2, ROI-3, ROI-4, etc.). Only the cell bodies in the closest proximity to the neuropil ROI were used in these tests (Fig. 5B,C). We identified 21 such "Neuropil-Soma" pairs of ROIs and included them in the numerical analysis (Fig. 5I, 500 Hz). ROIs corresponding to the neuropil and ROIs covering the surrounding cell bodies were selected using a spatial average of 57 pixels, covering an area of approximately $20 \times 20 \mu m$ in the object field. The optical traces were corrected for photobleaching by an exponential subtraction and filtered with low pass Gaussian (44 Hz cut off), and high pass RC (0.1 Hz). Traces exported from NeuroplexTM were opened in Clampfit for further adjustments of the baseline (if necessary) and only the Ca²⁺ spikes emerging 2 standard deviations above the baseline noise were counted. In total, we analyzed 6 ROIs positioned on the neuropil void of cell bodies, here dubbed "Neuropil-ROI". Each Neuropil-ROI was compared against 2-5 cell body ROIs (Soma-ROI) surrounding the Neuropil-ROI. We found a significantly greater number of events in the neuropil then in the cell body (21 ROI). The spike detection rate was consistently higher in the Neuropil-ROI compared to the Soma-ROI, with this difference being statistically significant (paired *t*-test, p < 0.01) (Fig. 5I, asterisks).

3.6 Dendritic Ca^{2+} Signals Exhibit Greater Amplitude and Faster Dynamics

 ${\rm Ca^{2+}}$ imaging allows real-time analysis of individual cells and subcellular compartments, such as dendrites [2]. We investigated spontaneous ${\rm Ca^{2+}}$ activity in dendrites of bulk-loaded neurons (OGB1-AM, Fig. 6). In visual fields recorded at 500 Hz (n = 14), we identified 10 cells with thick dendritic branches not obscured by neighboring cell bodies (Fig. 6A, Cells 1–3). In each of these neurons (10 out of 10), the dendritic optical signal exhibited greater amplitude and shorter duration than the corresponding somatic signal (Fig. 6A, compare optical traces "dend." vs. "soma").

Assuming that calcium influx and efflux occur only through calcium channels on the neuronal plasma membrane, and that these channels are uniformly distributed across various neuronal compartments (e.g., soma, dendrite), smaller compartments with a higher surface-to-volume ratio, such as dendrites, should exhibit larger calcium transients (greater amplitude) and higher calcium clearance rates (shorter half-width) than the cell bodies. However, the severe low-pass filtering of optical transients in the soma (Fig. 6A) suggests additional factors beyond the surface-to-volume ratio.

To further explore this, in the next series of experiments we recorded Ca²⁺ transients from two ROIs on opposite poles of the same cell body (Fig. 6B). One pole contained the cell nucleus ("Nucleus"), while the other pole, serving as a junction point to thick dendrites (presumably apical dendrites), had a conical shape ("Conus") (Fig. 6B). Despite two ROIs being positioned on the same cell body, less than 5 micrometers apart, their corresponding optical signals showed vastly different Ca²⁺ waveforms (Fig. 6B, right panel). Invariably, the ROIs positioned on the rounded part of the cell body showed smaller amplitude ($\Delta F/F$) and slower temporal dynamics compared to the ROIs positioned on the half of the cell body lacking the cell nucleus. Both "Nucleus" and "Conus" portions had similar diameters and therefore similar surface-to-volume ratios. We found significantly higher resting fluorescence F in the "Nucleus" compared to "Conus" (2259 \pm 62 a.u. vs. 1497 \pm 227 a.u., n = 58). As the F value may vary among coverslips, and even among neighboring cells on the same coverslip, we normalized "Conus F" by the corresponding "Nucleus F". We found that on average the fluorescence intensity of the cell body-conus was 67.5 ± 10.6 % of that found in the nucleus of the same cell (n = 57).

High-resolution IR-DIC photographs confirmed the presence of the cell nucleus in the rounded soma portion (Fig. 6B, IR-DIC), but this did not explain the stronger fluorescence from one half of the cell body. Subsequently, we transferred glass coverslips with bulk-loaded neurons from the Ca²⁺ imaging station (Fig. 6B) to a confocal microscope with a 40× water-immersion objective lens (Fig. 6C). In all examined neurons (n = 22), the cell body nucleus was notably brighter than the cytoplasm, indicating that the fluorescent dye was concentrated in the nucleus (Fig. 6C). This concentration inflates the resting fluorescence (F) without contributing to the fractional change (ΔF), thereby reducing the amplitude of the Ca^{2+} optical signal ($\Delta F/F$) in the "Nucleus" compared to the "Conus" (Fig. 6B). These data indicate that even minor variations in ROI selection on the same neuronal cell body can cause significant variations in optical signal amplitude and temporal dynamics.

3.7 Ca²⁺ Optical Signal Rise-Time and Duration

Numerical analysis was conducted on 35 neurons, where Ca^{2+} imaging sessions were performed at two distinct sampling rates. Each neuron's spontaneous electrical activity was monitored optically through Ca^{2+} imaging, first at 14 Hz and then at 500 Hz, with no changes in cell



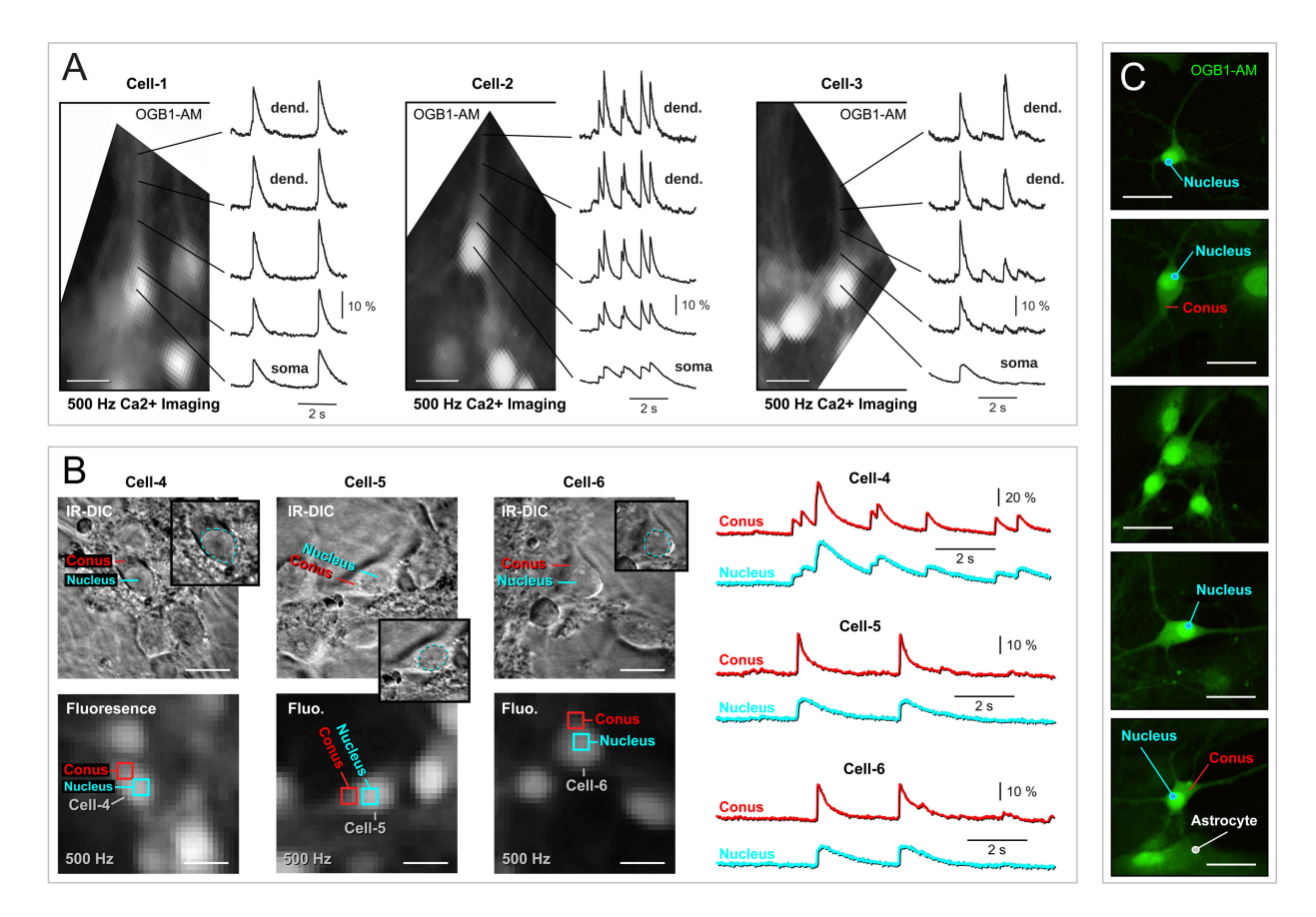


Fig. 6. Spontaneous dendritic Ca^{2+} signals exhibit greater amplitude and faster dynamics. (A) Neurons were bulk-loaded with Ca^{2+} sensitive dye OGB1-AM. Optical recordings of the spontaneous neuronal activity were acquired at 500 Hz sampling rate. Five regions of interest along the dendrite-soma junction are displayed next to the image of the cell obtained with a fast, low-resolution CCD camera. Three cells were selected for display (Cell-1, Cell-2, and Cell-3). (B) Prior to Ca^{2+} imaging, neurons were photographed using IR-DIC. The round part of the cell body contains the nucleus, while the conical part of the cell body does not. The scale bar is 20 μm. The magnification of the small image is 40x objective. Below the IR-DIC image, we show the same area captured by a fast CCD camera with low resolution (80 × 80 pixels), using a 500 Hz sampling rate. One ROI is selected on the cell nucleus (Nucleus), while the other ROI is on the part of the cell body without nucleus (Conus). Optical traces corresponding to these two ROIs (Conus and Nucleus) are displayed on the right side of this figure panel. Note a dramatic difference in the Ca^{2+} waveform for two neighboring ROIs. (C) In bulk-loaded neurons (OGB1-AM), confocal photographs reveal a higher concentration of the Ca^{2+} sensitive dye in the nucleus compared to the conus. Five examples are shown. The scale bar is 20 μm. IR-DIC, Infrared Differential Interference Contrast.

position (X-Y) or focus (Z) between recordings. The risetime of the optical signal, defined as the time taken to go from 10% to 90% of the maximum value, was quantified using Clampfit (Axon Instruments) (Fig. 7A).

Contrary to our initial visual assessment, which suggested that large, long-duration Ca²⁺ transients had similar waveforms at both 14 Hz and 500 Hz (Figs. 2,3), numerical analysis revealed significant differences. Specifically, the Ca²⁺ signal rise-time was markedly shorter (faster) in traces obtained at the higher sampling rate. At 14 Hz, the mean rise-time was 113.35 ± 5.36 ms (n = 35), while at 500 Hz, it was significantly faster, with a mean rise-time of 39.44 ± 3.36 ms (n = 35) (Fig. 7B). A paired *t*-test confirmed that the difference between 14 Hz and 500 Hz rise-times was statistically significant (p < 0.001).

Additionally, we quantified the duration of Ca^{2+} transients at half amplitude (half-width) (Fig. 7A). The half-widths of the Ca^{2+} signals also exhibited substantial differences between the two sampling rates. At 14 Hz, the mean half-width was 343.02 ± 21.79 ms (n = 35), whereas at 500 Hz, it was significantly shorter, with a mean half-width of 182.15 ± 28.07 ms (n = 35) (Fig. 7C). The difference in half-widths between the 14 Hz and 500 Hz data was statistically significant (paired *t*-test, p < 0.001). These findings highlight that higher sampling rates capture faster and shorter Ca^{2+} transients, indicating that lower sampling rates may miss critical temporal details of neuronal activity.



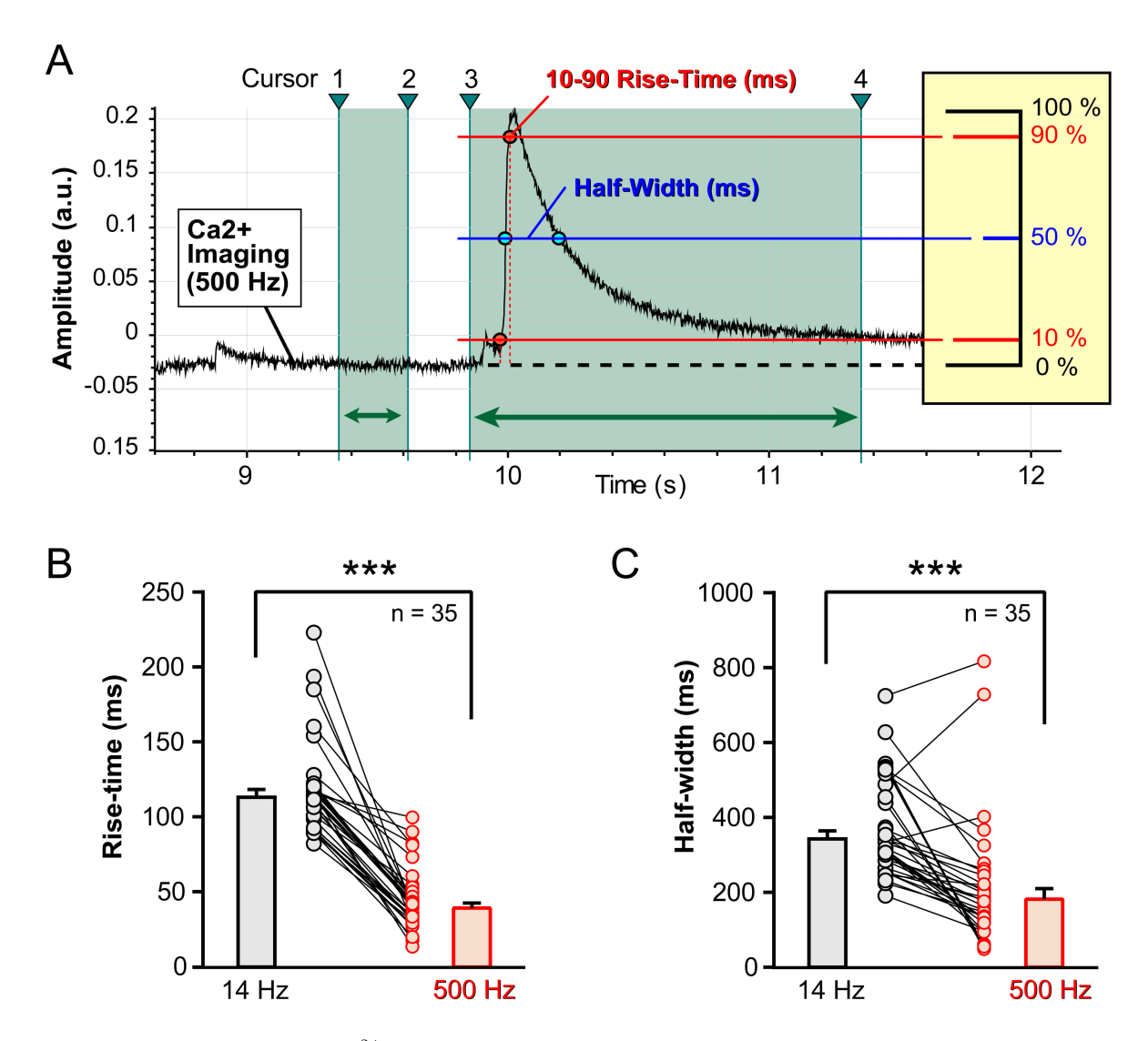


Fig. 7. Rise-time and duration. (A) A Ca^{2+} imaging trace, imported into Clampfit for quantification of the 10–90 Rise-Time and Half-Width. The trace segment between Cursor-1 and Cursor-2 is used for calculation of the "baseline". The trace segment between Cursor-3 and Cursor-4 is used for calculation of the "Rise-Time" and "Half-Width". Rise-Time is defined as the period of time required for an optical signal to climb from 10% to 90% of the peak amplitude (100%). Half-Width is defined as the duration of time between two blue points selected at the intersection of the Ca^{2+} trace and the 50% amplitude level (blue horizontal line). (B) Spontaneous Ca^{2+} events sampled in the same cell, first at 14 Hz and then at 500 Hz (paired Student's t-test, p < 0.001). (C) Same as in B, except half-widths are compared at two sampling rates. "n" is the number of individual cells analyzed. *** indicate p < 0.001.

3.8 Unbiased Extraction

We utilized EZcalcium, an open-source software with an intuitive graphical user interface (GUI) [45], to perform consistent analysis of Ca^{2+} imaging data across different visual fields (Fig. $8A_1$ – A_3). The software facilitated the extraction of optical traces corresponding to putative individual neurons (Fig. 8B), which were subsequently analyzed using a custom Python routine in Jupyter Lab. This routine detected and quantified Ca^{2+} transients, measuring their frequency (in Hz or per sweep), peak amplitude ($\Delta F/F$), and duration at half amplitude (half-width in milliseconds). When the same detection threshold was applied, both the manual and EZcalcium methods identified a simi-

lar number of Ca^{2+} transients, with no significant difference in the average count (unpaired Student's *t*-test, p=0.065) (Fig. 8C, Left). However, the transients identified by EZcalcium exhibited significantly smaller peak amplitudes (Fig. 8C, Middle) and notably longer durations (halfwidths) (Fig. 8C, Right) compared to those identified manually (unpaired Student's *t*-test, p<0.001 for both comparisons). These findings suggest that while EZcalcium is effective in detecting Ca^{2+} transients, it may differ from manual analysis in the sensitivity to signal amplitude and duration.



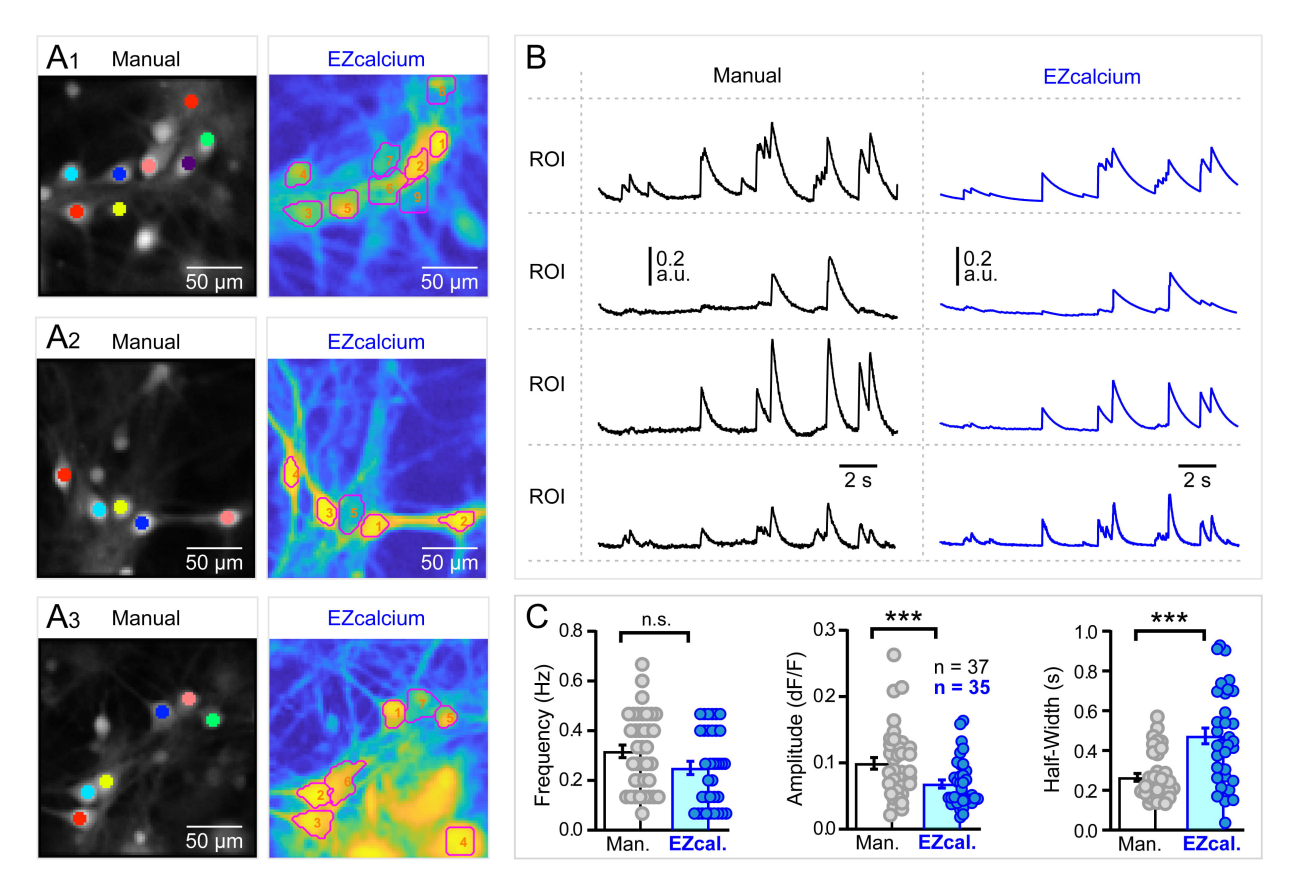


Fig. 8. Unbiased processing of the 500 Hz Ca²⁺ imaging data. (A) A₁–A₃ represent three examples of the same data (500 Hz Ca²⁺ imaging) analyzed in two ways: using the Manual approach (Left Image) and using the software routine *EZcalcium* (Right image). Manual approach employed ROIs of identical shape and size (37 pixels). The EZcalcium approach generated ROIs of irregular shape. The scale bar is 50 μ m. (B) Side by side comparison of optical traces obtained manually (black) versus EZcalcium (blue). The left column presents Ca²⁺ imaging traces from 4 regions of interest (ROIs) selected manually. The right column displays traces from the matching ROIs extracted using *EZcalcium*. The EZcalcium software reduces noise and determines the estimated timing of the Ca²⁺ transients (inferred). However, in this process, the optical signal amplitude appears reduced (compare black and blue traces). (C) We analyzed 4 experiments using both Manual and EZcalcium approaches. Each data point is one ROI. "n" – indicates the number of ROIs included in the analysis. From the same 4 fields of view (FOV), a similar number of spikes were detected using the two approaches (Frequency in Hz). From the same 4 FOVs, the EZcalcium approach assigned smaller amplitudes to the Ca²⁺ transients. The optical signal duration at half amplitude (Half-Width in ms) was significantly longer after processing of the optical data with the EZcalcium software. *** indicate p < 0.001; n.s. indicates, not significant, p > 0.05.

4. Discussion

4.1 Cultured Neurons as a Model for Neuronal Electrical Signaling

Primary neurons in culture serve as a useful experimental system for studying fundamental concepts in neuroscience [52], investigating disease mechanism [53,54]; and developing experimental strategies [55–57]. These neurons capture the essential elements of neuronal electrical signaling, primarily through excitatory postsynaptic potentials (EPSPs), inhibitory postsynaptic potentials (IPSPs) (Figs. 1E), and APs. After 10–12 days in culture, primary neurons develop membrane excitability sufficient to generate action potentials and form active synaptic connections [58]. A major advantage of cultured neurons is that they are

capable of forming active synaptic connections and generating electrical activity without external stimulation [59–61]. This unprovoked (spontaneous) electrical activity, which is also a feature present in both developing and mature brains [62], was used to study the properties of optical signals in Ca²⁺ imaging sessions (Figs. 1,2,3,4,5,6,7,8).

4.2 Mechanisms of Neuronal Ca²⁺ Transients

Fluorometric Ca^{2+} imaging is a sensitive method for monitoring neuronal activity [1,63]. Neuronal Ca^{2+} transients are primarily driven by depolarizing electrical signals that activate voltage-gated Ca^{2+} channels, leading to Ca^{2+} influx [1]. These signals are crucial for elementary forms of neuronal communication, such as chemical synaptic transmission, and may be further amplified by Ca^{2+} re-



lease from intracellular Ca^{2+} stores [64,65]. Thus, the amplitude of Ca^{2+} signals can be derived from three complementary sources: voltage-gated Ca^{2+} channels [2], Ca^{2+} permeable glutamate receptors [49], and release from internal Ca^{2+} stores [64,65].

4.3 Detection of Neuronal Ca²⁺ Transients

Ca²⁺-sensitive dyes are powerful tools for studying neural circuit dynamics at single-cell resolution [66]. In large-scale imaging applications, neuronal Ca²⁺ transients are often interpreted as APs, though the exact electrical signals associated with these transients are not always specified [8,67,68]. While bolus loading of membranepermeable calcium indicators allows for the simultaneous monitoring of hundreds of neurons [63], the signal-to-noise ratio (SNR) decreases in vivo due to fluorescence signal scattering by thick brain tissues, complicating single AP detection [69]. Additionally, the small surface-to-volume ratio in somatic compartments limits the detection of Ca²⁺ changes [69]. The likelihood of detecting a single AP in in vivo Ca²⁺ imaging is approximately 0.1 [68], while the detection rate for two successive APs could be 0.4, or lower. When optical recordings are paired with electrical recordings (e.g., whole cell) from the same neuron, then approximately 6 out of 10 events involving two consecutive APs in the electrical channel, resulted in no detectable changes in the Ca²⁺ imaging channel [68]. Interestingly, spikeless subthreshold depolarizations can sometimes generate detectable calcium transients [70–72].

4.4 Surface-to-Volume (STV) Ratio

Cells require a high surface to volume (STV) ratio to facilitate efficient chemical processes and the exchange of substances in and out of the cell. A higher STV ratio provides more surface area for substance exchange, typically resulting in a healthier cell. Smaller neuronal compartments have a greater STV ratio; for example, a dendritic branch has a higher STV ratio than the cell body. Several studies have found that during AP firing, calcium (Ca²⁺) signals are more pronounced in dendrites than in the cell body of the same neuron [2,73]. Additionally, AP-evoked Ca²⁺ transients are more prominent in single boutons compared to other subcellular compartments of layer 2/3 pyramidal cells [74]. In Aplysia ganglion, Ca²⁺ dye bulk loading showed that the increase in fluorescence following spike activity was larger in the axon hillock (the cell body conus) than in the middle of the cell body [75]. The increased fluorescence in the axon hillock compared to the cell body following spike activity further highlights the importance of STV ratio in Ca²⁺ dynamics.

4.5 Biphasic Decay of Ca²⁺ Transients

Smaller calcium transients evoked by single action potentials exhibit a mono-exponential decay. However, larger, and prolonged calcium transients, such as those evoked by trains of action potentials, display biphasic decay curves. Several mechanisms may account for this biphasic decay, including buffer non-linearities [76], calcium dependent regulation of calcium extrusion [77], intrinsic non-linearities in calcium transporters, and diffusion of calcium into adjacent compartments [74]. Although the precise mechanism remains unclear, its prevalence across various preparations and synapses suggests that biphasic decay is likely a physiological mechanism for calcium clearance following substantial Ca²⁺ influx.

4.6 Nuclear Effects on Optical Signals

A critical consideration in using chemical indicators like OGB1-AM is their accumulation in the cell nucleus, which can distort optical signal properties (Fig. 6A,B). The cell nucleus contains a nucleoplasmic reticulum capable of regulating Ca²⁺ fluctuations in localized subnuclear regions [78]. This intracellular machinery allows Ca²⁺ to simultaneously regulate various nuclear processes, linking neuronal activity to nuclear functions [78,79]. However, nuclear accumulation of Ca²⁺ indicators can lead to a loss of dynamic Ca²⁺ signaling and, eventually, to programmed cell death [80–82]. In neurons expressing GCaMP variants via adeno-associated virus (AAV) vectors, nuclear fluorescence can cause abnormal physiological responses, albeit without significant deficits in cortical circuits [3]. Dynamic Ca²⁺ signaling at the level of a neuronal nucleus has been shown to regulate the genetic program for neuroprotection and dendritic morphology [79,83].

4.7 Optical Crosstalk

In the current study, we used a well-established approach of manual ROI selection, where ROIs are placed on the cell bodies of individual neurons [54,84,85]. However, selected ROIs, and even single pixels, can contain a complex mixture of signals from neuropil, neurons, glial cells, and noise [86] that contaminate optical traces. We found that ROIs placed over areas containing dendrites and axons (i.e., neuropil) more frequently detected small-amplitude short-duration Ca²⁺ events, compared to ROIs containing cell bodies (Fig. 5). Apart from being an informative parameter in physiological studies, the observed difference can potentially be used for training automated ROI extraction models [45]. Importantly, the detection of sharp Ca²⁺ events in the neuropil required a fast optical sampling rate of 500 Hz. At the lower sampling frequency (14 Hz), sharp Ca²⁺ events were not detectable in the neuropil. This finding may explain why in vivo studies with optical sampling rates below 50 Hz often miss distinct neuropil Ca²⁺ dynamics (Fig. 5). Furthermore, experimental approaches based on the AM-ester conjugated Ca²⁺ indicators (e.g., OGB1-AM), generally fail to highlight neuronal dendrites, or fine glial processes due to low contrast. These small structures do not stand out with sharp contrast and cannot be readily delineated by morphological filtering [86].



4.8 Neuronal Identity

In single unit electrode recordings, the shape of an AP can be used to assign identities to neurons. Usually, such spike-sorting is based on the AP duration, where the fastest spikes come from inhibitory interneurons, and the slowest spikes are contributed by cortical pyramidal cells. However, Ca²⁺ activity waveforms do not provide strong signatures of individual cells' identities because the Ca²⁺ optical signals are strongly dictated by intracellular Ca²⁺ buffering and the dye's binding kinetics [87].

4.9 Demixing Strategies for Signal Extraction

In Ca²⁺ imaging data, selected ROIs and even single pixels can contain complex mixtures of signals originating from target neurons, weakly labeled or out-of-focus cell bodies, neuropil, astrocytes, and noise. Significant crosstalk is particularly the case when imaging with low spatial resolution to improve temporal resolution (Fig. 5), or when constrained by the equipment for in vivo calcium imaging (Tables 1,2). Disentangling these signals without suffering crosstalk and finding the precise locations and shapes of individual neurons requires intensive demixing strategies [86,88]. Demixing strategies for extraction of individual neurons from raw Ca2+ movies can be based on independent components analysis (ICA), non-negative matrix factorization (NMF), and constrained non-negative matrix factorization (CNMF). By using these demixing strategies, researchers can simultaneously infer the geometry and activity dynamics of specific neurons [45,86,88–91].

Here, we used an open-source toolbox (EZcalcium) for analysis of Ca²⁺ imaging data (Fig. 8) based on CNMF to differentiate between changes in fluorescence intensity that correspond to biological Ca²⁺ signals and differentiate from noise [45]. The advantage of EZcalcium is its intuitive GUI and easy inspection of traces and ROI shapes. In the current study, the sets of ROIs recognized by the EZcalcium program were similar to the manually extracted ROIs (Fig. 8A₁-A₃,B). The numbers of Ca²⁺ transients detected through unbiased ROI selection (EZcalcium) were similar to those obtained through manual ROI selection (Fig. 8C, Frequency). However, two fundamental parameters of spontaneous signals (peak amplitude and duration) were significantly different between the two approaches (Fig. 8C, Amplitude, Half-Width). These findings underscore that neural activity properties inferred from multi-cell Ca²⁺ imaging are highly dependent on the chosen event recovery methods, consistent with a previous study [92].

5. Conclusions

Our data reveal five distinct types of information that are easily lost in Ca²⁺ imaging studies due to optical undersampling. As expected, undersampling of large-amplitude Ca²⁺ transients leads to distortions in both (i) signal risetime and (ii) signal duration (half-width). However, several unexpected consequences were also identified: (iii) failure

to detect small-amplitude transients in cell bodies and (iv) omission of small-amplitude transients in the neuropil (axons and dendrites). Furthermore, we found that (v) including the cell nucleus within the region of interest (ROI) results in significant distortions of somatic Ca²⁺ transients. Specifically, two ROIs placed on the same cell body produced markedly different Ca²⁺ signals when one of the ROIs encompassed the nucleus.

Availability of Data and Materials

The datasets used and/or analyzed during the current study are available from the corresponding author on reasonable request.

Author Contributions

SDA, PRA and KDM designed research. TNB, CAV, YMDZ maintained the mouse colony. KDM and VOI developed cultured neurons. KDM, VOI, CAV, YMDZ, and SDA performed calcium imaging. KDM, VOI, and SDA analyzed data. KDM, PRA, and SDA wrote the paper. All authors contributed to editorial changes in the manuscript. All authors read and approved the final manuscript. All authors have participated sufficiently in the work and agreed to be accountable for all aspects of the work.

Ethics Approval and Consent to Participate

Euthanized mice were used for preparation of primary neuronal cultures, under the approval of the UConn Health Institutional Animal Care and Use Committee (IACUC), animal protocol (#200902).

Acknowledgment

We are grateful to John Glynn (UConn Health) and Chun Bleau (RedShirtImaging) and for technical support.

Funding

This research was funded by the Cure Alzheimer's Fund (#65539), the National Institute of Mental Health (U01MH109091), the National Institute on Aging (AG064554), the UConn Health Alcohol Research Center (ARC)/Kasowitz Medical Research Fund (P50AA027055), UConn IBACS Seed Grant, the H2020-MSCA-RISE-2017 (#778405), and Grant #4242 "NIMOCHIP" Science Fund RS.

Conflict of Interest

The authors declare no conflict of interest.

References

- [1] Ross WN. Changes in intracellular calcium during neuron activity. Annual Review of Physiology. 1989; 51: 491–506. https://doi.org/10.1146/annurev.ph.51.030189.002423
- [2] Jaffe DB, Johnston D, Lasser-Ross N, Lisman JE, Miyakawa H, Ross WN. The spread of Na+ spikes determines the pattern of



- dendritic Ca2+ entry into hippocampal neurons. Nature. 1992; 357: 244–246. https://doi.org/10.1038/357244a0
- [3] Chen TW, Wardill TJ, Sun Y, Pulver SR, Renninger SL, Baohan A, *et al.* Ultrasensitive fluorescent proteins for imaging neuronal activity. Nature. 2013; 499: 295–300. https://doi.org/10.1038/nature12354
- [4] Waters J. Sources of widefield fluorescence from the brain. eLife. 2020; 9: e59841. https://doi.org/10.7554/eLife.59841
- [5] Evans SW, Shi DQ, Chavarha M, Plitt MH, Taxidis J, Madruga B, et al. A positively tuned voltage indicator for extended electrical recordings in the brain. Nature Methods. 2023; 20: 1104–1113. https://doi.org/10.1038/s41592-023-01913-z
- [6] Song C, Do QB, Antic SD, Knöpfel T. Transgenic Strategies for Sparse but Strong Expression of Genetically Encoded Voltage and Calcium Indicators. International Journal of Molecular Sciences. 2017; 18: 1461. https://doi.org/10.3390/ijms18071461
- [7] Gradinaru V. Expanding the brain researcher's toolkit. Science. 2020; 369: 637. https://doi.org/10.1126/science.abd2660
- [8] Liang B, Zhang L, Barbera G, Fang W, Zhang J, Chen X, et al. Distinct and Dynamic ON and OFF Neural Ensembles in the Prefrontal Cortex Code Social Exploration. Neuron. 2018; 100: 700–714.e9. https://doi.org/10.1016/j.neuron.2018.08.043
- [9] Grienberger C, Giovannucci A, Zeiger W, Portera-Cailliau C. Two-photon calcium imaging of neuronal activity. Nature Reviews. Methods Primers. 2022; 2: 67. https://doi.org/10.1038/s43586-022-00147-1
- [10] Svoboda K, Yasuda R. Principles of two-photon excitation microscopy and its applications to neuroscience. Neuron. 2006; 50: 823–839. https://doi.org/10.1016/j.neuron.2006.05.019
- [11] Cardin JA, Crair MC, Higley MJ. Mesoscopic Imaging: Shining a Wide Light on Large-Scale Neural Dynamics. Neuron. 2020; 108: 33–43. https://doi.org/10.1016/j.neuron.2020.09.031
- [12] Oheim M, Beaurepaire E, Chaigneau E, Mertz J, Charpak S. Two-photon microscopy in brain tissue: parameters influencing the imaging depth. Journal of Neuroscience Methods. 2001; 111: 29–37. https://doi.org/10.1016/s0165-0270(01)00438-1
- [13] Helmchen F, Denk W. Deep tissue two-photon microscopy. Nature Methods. 2005; 2: 932–940. https://doi.org/10.1038/nmet
- [14] Sofroniew NJ, Flickinger D, King J, Svoboda K. A large field of view two-photon mesoscope with subcellular resolution for in vivo imaging. eLife. 2016; 5: e14472. https://doi.org/10.7554/ eLife.14472
- [15] Musall S, Kaufman MT, Juavinett AL, Gluf S, Churchland AK. Single-trial neural dynamics are dominated by richly varied movements. Nature Neuroscience. 2019; 22: 1677–1686. https://doi.org/10.1038/s41593-019-0502-4
- [16] Liu J, He Y, Lavoie A, Bouvier G, Liu BH. A direction-selective cortico-brainstem pathway adaptively modulates innate behaviors. Nature Communications. 2023; 14: 8467. https://doi.org/ 10.1038/s41467-023-42910-2
- [17] Tang L, Higley MJ. Layer 5 Circuits in V1 Differentially Control Visuomotor Behavior. Neuron. 2020; 105: 346–354.e5. https://doi.org/10.1016/j.neuron.2019.10.014
- [18] Heintz TG, Hinojosa AJ, Dominiak SE, Lagnado L. Opposite forms of adaptation in mouse visual cortex are controlled by distinct inhibitory microcircuits. Nature Communications. 2022; 13: 1031. https://doi.org/10.1038/s41467-022-28635-8
- [19] Allen WE, Kauvar IV, Chen MZ, Richman EB, Yang SJ, Chan K, *et al.* Global Representations of Goal-Directed Behavior in Distinct Cell Types of Mouse Neocortex. Neuron. 2017; 94: 891–907.e6. https://doi.org/10.1016/j.neuron.2017.04.017
- [20] Liu J, Whiteway MR, Sheikhattar A, Butts DA, Babadi B, Kanold PO. Parallel Processing of Sound Dynamics across Mouse Auditory Cortex via Spatially Patterned Thalamic Inputs and Distinct Areal Intracortical Circuits. Cell Reports. 2019; 27:

- 872-885.e7. https://doi.org/10.1016/j.celrep.2019.03.069
- [21] Musall S, Sun XR, Mohan H, An X, Gluf S, Li SJ, et al. Pyramidal cell types drive functionally distinct cortical activity patterns during decision-making. Nature Neuroscience. 2023; 26: 495–505. https://doi.org/10.1038/s41593-022-01245-9
- [22] Keller AJ, Dipoppa M, Roth MM, Caudill MS, Ingrosso A, Miller KD, et al. A Disinhibitory Circuit for Contextual Modulation in Primary Visual Cortex. Neuron. 2020; 108: 1181– 1193.e8. https://doi.org/10.1016/j.neuron.2020.11.013
- [23] Ren C, Peng K, Yang R, Liu W, Liu C, Komiyama T. Global and subtype-specific modulation of cortical inhibitory neurons regulated by acetylcholine during motor learning. Neuron. 2022; 110: 2334–2350.e8. https://doi.org/10.1016/j.neuron.2022.04. 031
- [24] Benisty H, Barson D, Moberly AH, Lohani S, Tang L, Coifman RR, et al. Rapid fluctuations in functional connectivity of cortical networks encode spontaneous behavior. Nature Neuroscience. 2024; 27: 148–158. https://doi.org/10.1038/s41593-023-01498-y
- [25] Ferguson KA, Salameh J, Alba C, Selwyn H, Barnes C, Lohani S, et al. VIP interneurons regulate cortical size tuning and visual perception. Cell Reports. 2023; 42: 113088. https://doi.org/10.1016/j.celrep.2023.113088
- [26] Gasselin C, Hohl B, Vernet A, Crochet S, Petersen CCH. Cell-type-specific nicotinic input disinhibits mouse barrel cortex during active sensing. Neuron. 2021; 109: 778–787.e3. https://doi.org/10.1016/j.neuron.2020.12.018
- [27] Korzhova V, Marinković P, Njavro JR, Goltstein PM, Sun F, Tahirovic S, et al. Long-term dynamics of aberrant neuronal activity in awake Alzheimer's disease transgenic mice. Communications Biology. 2021; 4: 1368. https://doi.org/10.1038/ s42003-021-02884-7
- [28] He CX, Cantu DA, Mantri SS, Zeiger WA, Goel A, Portera-Cailliau C. Tactile Defensiveness and Impaired Adaptation of Neuronal Activity in the *Fmr1* Knock-Out Mouse Model of Autism. The Journal of Neuroscience. 2017; 37: 6475–6487. https://doi.org/10.1523/JNEUROSCI.0651-17.2017
- [29] Ren C, Komiyama T. Wide-field calcium imaging of cortexwide activity in awake, head-fixed mice. STAR Protocols. 2021; 2: 100973. https://doi.org/10.1016/j.xpro.2021.100973
- [30] Smith GB, Hein B, Whitney DE, Fitzpatrick D, Kaschube M. Distributed network interactions and their emergence in developing neocortex. Nature Neuroscience. 2018; 21: 1600–1608. https://doi.org/10.1038/s41593-018-0247-5
- [31] Wang H, Flores RJ, Yarur HE, Limoges A, Bravo-Rivera H, Casello SM, et al. Prefrontal cortical dynorphin peptidergic transmission constrains threat-driven behavioral and network states. Neuron. 2024; 112: 2062–2078.e7. https://doi.org/10. 1016/j.neuron.2024.03.015
- [32] Ishino S, Kamada T, Sarpong GA, Kitano J, Tsukasa R, Mukohira H, et al. Dopamine error signal to actively cope with lack of expected reward. Science Advances. 2023; 9: eade5420. https://doi.org/10.1126/sciadv.ade5420
- [33] Rynes ML, Surinach DA, Linn S, Laroque M, Rajendran V, Dominguez J, et al. Miniaturized head-mounted microscope for whole-cortex mesoscale imaging in freely behaving mice. Nature Methods. 2021; 18: 417–425. https://doi.org/10.1038/ s41592-021-01104-8
- [34] Nietz AK, Popa LS, Streng ML, Carter RE, Kodandaramaiah SB, Ebner TJ. Wide-Field Calcium Imaging of Neuronal Network Dynamics In Vivo. Biology. 2022; 11: 1601. https://doi.or g/10.3390/biology11111601
- [35] Heiss JE, Zhong P, Lee SM, Yamanaka A, Kilduff TS. Distinct lateral hypothalamic CaMKIIα neuronal populations regulate wakefulness and locomotor activity. Proceedings of the National Academy of Sciences of the United States of America. 2024;



- 121: e2316150121. https://doi.org/10.1073/pnas.2316150121
- [36] Lohani S, Moberly AH, Benisty H, Landa B, Jing M, Li Y, et al. Spatiotemporally heterogeneous coordination of cholinergic and neocortical activity. Nature Neuroscience. 2022; 25: 1706–1713. https://doi.org/10.1038/s41593-022-01202-6
- [37] Piantadosi SC, Manning EE, Chamberlain BL, Hyde J, La-Palombara Z, Bannon NM, *et al.* Hyperactivity of indirect pathway-projecting spiny projection neurons promotes compulsive behavior. Nature Communications. 2024; 15: 4434. https://doi.org/10.1038/s41467-024-48331-z
- [38] Manning EE, Geramita MA, Piantadosi SC, Pierson JL, Ahmari SE. Distinct Patterns of Abnormal Lateral Orbitofrontal Cortex Activity During Compulsive Grooming and Reversal Learning Normalize After Fluoxetine. Biological Psychiatry. 2023; 93: 989–999. https://doi.org/10.1016/j.biopsych.2021.11.018
- [39] Liu X, Ren C, Lu Y, Liu Y, Kim JH, Leutgeb S, et al. Multimodal neural recordings with Neuro-FITM uncover diverse patterns of cortical-hippocampal interactions. Nature Neuroscience. 2021; 24: 886–896. https://doi.org/10.1038/s41593-021-00841-5
- [40] Makino H, Ren C, Liu H, Kim AN, Kondapaneni N, Liu X, et al. Transformation of Cortex-wide Emergent Properties during Motor Learning. Neuron. 2017; 94: 880–890.e8. https://doi.org/10.1016/j.neuron.2017.04.015
- [41] Chen Y, Jang H, Spratt PWE, Kosar S, Taylor DE, Essner RA, et al. Soma-Targeted Imaging of Neural Circuits by Ribosome Tethering. Neuron. 2020; 107: 454–469.e6. https://doi.org/10. 1016/j.neuron.2020.05.005
- [42] Shemesh OA, Linghu C, Piatkevich KD, Goodwin D, Celiker OT, Gritton HJ, et al. Precision Calcium Imaging of Dense Neural Populations via a Cell-Body-Targeted Calcium Indicator. Neuron. 2020; 107: 470–486.e11. https://doi.org/10.1016/j.neuron.2020.05.029
- [43] Robbins M, Christensen CN, Kaminski CF, Zlatic M. Calcium imaging analysis - how far have we come? F1000Research. 2021; 10: 258. https://doi.org/10.12688/f1000research.51755.2
- [44] Liu W, Pan J, Xu Y, Wang M, Jia H, Zhang K, et al. Fast and Accurate Motion Correction for Two-Photon Ca²⁺ Imaging in Behaving Mice. Frontiers in Neuroinformatics. 2022; 16: 851188. https://doi.org/10.3389/fninf.2022.851188
- [45] Cantu DA, Wang B, Gongwer MW, He CX, Goel A, Suresh A, et al. EZcalcium: Open-Source Toolbox for Analysis of Calcium Imaging Data. Frontiers in Neural Circuits. 2020; 14: 25. https://doi.org/10.3389/fncir.2020.00025
- [46] Spellman T, Svei M, Kaminsky J, Manzano-Nieves G, Liston C. Prefrontal deep projection neurons enable cognitive flexibility via persistent feedback monitoring. Cell. 2021; 184: 2750–2766.e17. https://doi.org/10.1016/j.cell.2021.03.047
- [47] Grødem S, Nymoen I, Vatne GH, Rogge FS, Björnsdóttir V, Lensjø KK, et al. An updated suite of viral vectors for in vivo calcium imaging using intracerebral and retro-orbital injections in male mice. Nature Communications. 2023; 14: 608. https: //doi.org/10.1038/s41467-023-36324-3
- [48] Ait Ouares K, Canepari M. The Origin of Physiological Local mGluR1 Supralinear Ca²⁺ Signals in Cerebellar Purkinje Neurons. The Journal of Neuroscience. 2020; 40: 1795–1809. https://doi.org/10.1523/JNEUROSCI.2406-19.2020
- [49] Milojkovic BA, Zhou WL, Antic SD. Voltage and calcium transients in basal dendrites of the rat prefrontal cortex. The Journal of Physiology. 2007; 585: 447–468. https://doi.org/10.1113/jphysiol.2007.142315
- [50] Kerlin A, Mohar B, Flickinger D, MacLennan BJ, Dean MB, Davis C, et al. Functional clustering of dendritic activity during decision-making. eLife. 2019; 8: e46966. https://doi.org/10. 7554/eLife.46966
- [51] TAUC L. Identification of active membrane areas in the giant neuron of Aplysia. The Journal of General Physiology. 1962;

- 45: 1099-1115. https://doi.org/10.1085/jgp.45.6.1099
- [52] Martinelli DC, Chew KS, Rohlmann A, Lum MY, Ressl S, Hattar S, et al. Expression of C1ql3 in Discrete Neuronal Populations Controls Efferent Synapse Numbers and Diverse Behaviors. Neuron. 2016; 91: 1034–1051. https://doi.org/10.1016/j.neuron.2016.07.002
- [53] Elamin M, Lemtiri-Chlieh F, Robinson TM, Levine ES. Dysfunctional sodium channel kinetics as a novel epilepsy mechanism in chromosome 15q11-q13 duplication syndrome. Epilepsia. 2023; 64: 2515–2527. https://doi.org/10.1111/epi.17687
- [54] Kapadia M, Bijelić D, Zhao H, Ma D, Stojanovich L, Milošević M, et al. Effects of sustained i.c.v. infusion of lupus CSF and autoantibodies on behavioral phenotype and neuronal calcium signaling. Acta Neuropathologica Communications. 2017; 5: 70. https://doi.org/10.1186/s40478-017-0473-1
- [55] Monakhov MV, Matlashov ME, Colavita M, Song C, Shcherbakova DM, Antic SD, et al. Screening and Cellular Characterization of Genetically Encoded Voltage Indicators Based on Near-Infrared Fluorescent Proteins. ACS Chemical Neuroscience. 2020; 11: 3523–3531. https://doi.org/10.1021/acschemneuro.0c00046
- [56] Bloxham B, Brinks D, Kheifets S, Cohen AE. Linearly polarized excitation enhances signals from fluorescent voltage indicators. Biophysical Journal. 2021; 120: 5333–5342. https://doi.org/10. 1016/j.bpj.2021.10.028
- [57] Puppo F, Sadegh S, Trujillo CA, Thunemann M, Campbell EP, Vandenberghe M, et al. All-Optical Electrophysiology in hiPSC-Derived Neurons With Synthetic Voltage Sensors. Frontiers in Cellular Neuroscience. 2021; 15: 671549. https://doi.org/10. 3389/fncel.2021.671549
- [58] Belinsky GS, Moore AR, Short SM, Rich MT, Antic SD. Physiological properties of neurons derived from human embryonic stem cells using a dibutyryl cyclic AMP-based protocol. Stem Cells and Development. 2011; 20: 1733–1746. https://doi.org/10.1089/scd.2010.0501
- [59] Suresh J, Radojicic M, Pesce LL, Bhansali A, Wang J, Tryba AK, et al. Network burst activity in hippocampal neuronal cultures: the role of synaptic and intrinsic currents. Journal of Neurophysiology. 2016; 115: 3073–3089. https://doi.org/10.1152/jn.00995.2015
- [60] Chubakov AR, Nikonov AA, Gromova EA. Impulse activity of cultured rat cerebral cortex neurons. Neirofiziologiia. 1975; 7: 581–588. (In Russian)
- [61] Cohen E, Ivenshitz M, Amor-Baroukh V, Greenberger V, Segal M. Determinants of spontaneous activity in networks of cultured hippocampus. Brain Research. 2008; 1235: 21–30. https://doi.org/10.1016/j.brainres.2008.06.022
- [62] Meyer-Baese L, Watters H, Keilholz S. Spatiotemporal patterns of spontaneous brain activity: a mini-review. Neurophotonics. 2022; 9: 032209. https://doi.org/10.1117/1.NPh.9.3.032209
- [63] Stosiek C, Garaschuk O, Holthoff K, Konnerth A. In vivo two-photon calcium imaging of neuronal networks. Proceedings of the National Academy of Sciences of the United States of America. 2003; 100: 7319–7324. https://doi.org/10.1073/pnas .1232232100
- [64] Nakamura T, Barbara JG, Nakamura K, Ross WN. Synergistic release of Ca2+ from IP3-sensitive stores evoked by synaptic activation of mGluRs paired with backpropagating action potentials. Neuron. 1999; 24: 727–737. https://doi.org/10.1016/ s0896-6273(00)81125-3
- [65] Emptage N, Bliss TV, Fine A. Single synaptic events evoke NMDA receptor-mediated release of calcium from internal stores in hippocampal dendritic spines. Neuron. 1999; 22: 115– 124. https://doi.org/10.1016/s0896-6273(00)80683-2
- [66] Grewe BF, Helmchen F. Optical probing of neuronal ensemble activity. Current Opinion in Neurobiology. 2009; 19: 520–529.



- https://doi.org/10.1016/j.conb.2009.09.003
- [67] Deneux T, Kaszas A, Szalay G, Katona G, Lakner T, Grinvald A, et al. Accurate spike estimation from noisy calcium signals for ultrafast three-dimensional imaging of large neuronal populations in vivo. Nature Communications. 2016; 7: 12190. https://doi.org/10.1038/ncomms12190
- [68] de Vries SEJ, Lecoq JA, Buice MA, Groblewski PA, Ocker GK, Oliver M, et al. A large-scale standardized physiological survey reveals functional organization of the mouse visual cortex. Nature Neuroscience. 2020; 23: 138–151. https://doi.org/10.1038/ s41593-019-0550-9
- [69] Tada M, Takeuchi A, Hashizume M, Kitamura K, Kano M. A highly sensitive fluorescent indicator dye for calcium imaging of neural activity in vitro and in vivo. The European Journal of Neuroscience. 2014; 39: 1720–1728. https://doi.org/10.1111/ej n.12476
- [70] Murphy TH, Blatter LA, Wier WG, Baraban JM. Spontaneous synchronous synaptic calcium transients in cultured cortical neurons. The Journal of Neuroscience. 1992; 12: 4834–4845. https://doi.org/10.1523/JNEUROSCI.12-12-04834.1992
- [71] Bandyopadhyay S, Shamma SA, Kanold PO. Dichotomy of functional organization in the mouse auditory cortex. Nature Neuroscience. 2010; 13: 361–368. https://doi.org/10.1038/nn .2490
- [72] Milicevic KD, Ivanova VO, Lovic DD, Platisa J, Andjus PR, Antic SD. Plateau depolarizations in spontaneously active neurons detected by calcium or voltage imaging. Scientific Reports. 2024; 14: 22787. https://doi.org/10.1038/s41598-024-70319-4
- [73] Svoboda K, Denk W, Kleinfeld D, Tank DW. In vivo dendritic calcium dynamics in neocortical pyramidal neurons. Nature. 1997; 385: 161–165. https://doi.org/10.1038/385161a0
- [74] Koester HJ, Sakmann B. Calcium dynamics associated with action potentials in single nerve terminals of pyramidal cells in layer 2/3 of the young rat neocortex. The Journal of Physiology. 2000; 529: 625–646. https://doi.org/10.1111/j.1469-7793.2000. 00625.x
- [75] Yoshida R, Iwamoto A, Nagahama T. Calcium Imaging for Detection and Estimation of Spike Activities in Aplysia Neurons. Zoological Science. 2001; 18: 631–643. https://doi.org/ 10.2108/zsj.18.631
- [76] Tank DW, Regehr WG, Delaney KR. A quantitative analysis of presynaptic calcium dynamics that contribute to short-term enhancement. The Journal of Neuroscience. 1995; 15: 7940–7952. https://doi.org/10.1523/JNEUROSCI.15-12-07940.1995
- [77] Scheuss V, Yasuda R, Sobczyk A, Svoboda K. Nonlinear [Ca2+] signaling in dendrites and spines caused by activity-dependent depression of Ca2+ extrusion. The Journal of Neuroscience. 2006; 26: 8183–8194. https://doi.org/10.1523/JNEUROSCI. 1962-06 2006
- [78] Echevarría W, Leite MF, Guerra MT, Zipfel WR, Nathanson MH. Regulation of calcium signals in the nucleus by a nucle-oplasmic reticulum. Nature Cell Biology. 2003; 5: 440–446. https://doi.org/10.1038/ncb980
- [79] Bading H. Nuclear calcium signalling in the regulation of brain

- function. Nature Reviews. Neuroscience. 2013; 14: 593–608. https://doi.org/10.1038/nrn3531
- [80] Tian L, Hires SA, Mao T, Huber D, Chiappe ME, Chalasani SH, et al. Imaging neural activity in worms, flies and mice with improved GCaMP calcium indicators. Nature Methods. 2009; 6: 875–881. https://doi.org/10.1038/nmeth.1398
- [81] Grienberger C, Konnerth A. Imaging calcium in neurons. Neuron. 2012; 73: 862–885. https://doi.org/10.1016/j.neuron.2012.02.011
- [82] Gasterstädt I, Jack A, Stahlhut T, Rennau LM, Gonda S, Wahle P. Genetically Encoded Calcium Indicators Can Impair Dendrite Growth of Cortical Neurons. Frontiers in Cellular Neuroscience. 2020; 14: 570596. https://doi.org/10.3389/fncel.2020.570596
- [83] Zhang SJ, Zou M, Lu L, Lau D, Ditzel DAW, Delucinge-Vivier C, et al. Nuclear calcium signaling controls expression of a large gene pool: identification of a gene program for acquired neuroprotection induced by synaptic activity. PLoS Genetics. 2009; 5: e1000604. https://doi.org/10.1371/journal.pgen.1000604
- [84] Dombeck DA, Khabbaz AN, Collman F, Adelman TL, Tank DW. Imaging large-scale neural activity with cellular resolution in awake, mobile mice. Neuron. 2007; 56: 43–57. https://doi.org/10.1016/j.neuron.2007.08.003
- [85] Greenberg DS, Houweling AR, Kerr JND. Population imaging of ongoing neuronal activity in the visual cortex of awake rats. Nature Neuroscience. 2008; 11: 749–751. https://doi.org/10.1038/nn.2140
- [86] Mukamel EA, Nimmerjahn A, Schnitzer MJ. Automated analysis of cellular signals from large-scale calcium imaging data. Neuron. 2009; 63: 747–760. https://doi.org/10.1016/j.neuron.2009.08.009
- [87] Helmchen F, Imoto K, Sakmann B. Ca2+ buffering and action potential-evoked Ca2+ signaling in dendrites of pyramidal neurons. Biophysical Journal. 1996; 70: 1069–1081. https://doi.org/10.1016/S0006-3495(96)79653-4
- [88] Pnevmatikakis EA, Soudry D, Gao Y, Machado TA, Merel J, Pfau D, et al. Simultaneous Denoising, Deconvolution, and Demixing of Calcium Imaging Data. Neuron. 2016; 89: 285–299. https://doi.org/10.1016/j.neuron.2015.11.037
- [89] Maruyama R, Maeda K, Moroda H, Kato I, Inoue M, Miyakawa H, et al. Detecting cells using non-negative matrix factorization on calcium imaging data. Neural Networks. 2014; 55: 11–19. https://doi.org/10.1016/j.neunet.2014.03.007
- [90] Friedrich J, Giovannucci A, Pnevmatikakis EA. Online analysis of microendoscopic 1-photon calcium imaging data streams. PLoS Computational Biology. 2021; 17: e1008565. https://doi.org/10.1371/journal.pcbi.1008565
- [91] Giovannucci A, Friedrich J, Gunn P, Kalfon J, Brown BL, Koay SA, et al. CaImAn an open source tool for scalable calcium imaging data analysis. eLife. 2019; 8: e38173. https://doi.org/ 10.7554/eLife.38173
- [92] Evans MH, Petersen RS, Humphries MD. On the use of calcium deconvolution algorithms in practical contexts. bioRxiv. 2019; 871137. (preprint) https://doi.org/10.1101/871137

